Journal of Nanobiotechnology

RESEARCH

Open Access

Oral administration of *Momordica charantia*-derived extracellular vesicles alleviates ulcerative colitis through comprehensive renovation of the intestinal microenvironment

Bowen Gao[1†], Xiaoling Huang[2†], Junlong Fu[1], Liyuan Chen[1], Zhichao Deng[1], Shuhui Wang[3], Yuanyuan Zhu[1], Chenxi Xu[1], Yujie Zhang[1], Mingxin Zhang[4], Lina Chen[1], Manli Cui[4*] and Mingzhen Zhang[1*]

Abstract

Background Ulcerative colitis (UC) is an inflammatory bowel disease (IBD), accompanied by intense inflammation, oxidative stress, and intestinal microbiota dysbiosis. Current treatments using chemotherapeutic drugs or immunosuppressants have limited effectiveness and side effects. Therefore, the development of safe, effective, and multi-targeting therapies for IBD is of great importance. *Momordica charantia* exhibits antioxidant, anti-inflammatory, and intestinal microbiota-regulating properties, suggesting that *Momordica charantia*-derived extracellular vesicles (MCEVs) have the potential for UC management.

Results We extracted MCEVs using differential centrifugation and density gradient centrifugation. The results showed that MCEVs possessed high purity, even particle size, and excellent stability. In vitro, MCEVs were shown to inhibit macrophage inflammatory responses, scavenge reactive oxygen species (ROS), and protect cells from oxidative damage. Transcriptomics analysis revealed that MCEVs may alleviate mitochondria-dependent apoptosis by safeguarding the integrity of the mitochondrial structure and regulating the expression of apoptosis-related proteins. Furthermore, all components of MCEVs contributed to their pharmacological activity. In vivo, MCEVs had better retention in the inflamed colon and significantly alleviated UC through a comprehensive renovation of the intestinal microenvironment.

Conclusion These findings suggested that MCEVs own considerable potential as natural nanotherapeutics for UC treatment.

†Bowen Gao and Xiaoling Huang contributed equally to this work.

*Correspondence:
Manli Cui
cuiml1587@163.com
Mingzhen Zhang
mzhang21@xjtu.edu.cn

Full list of author information is available at the end of the article

Graphical abstract

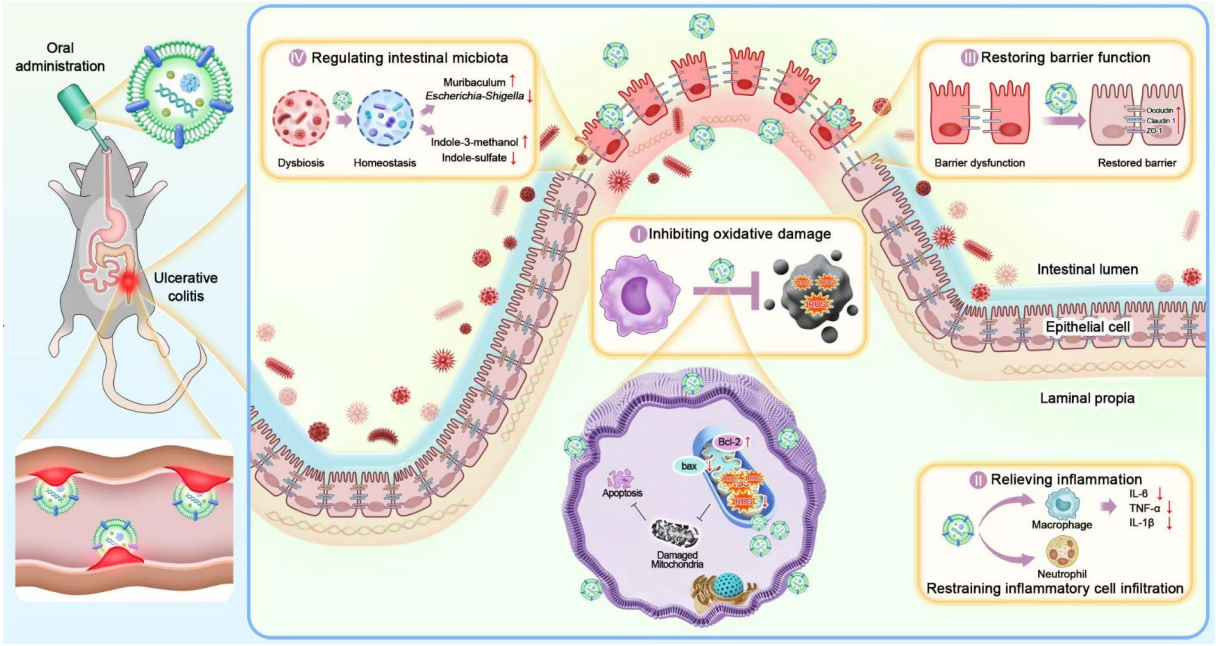

Keywords Ulcerative colitis, *Momordica charantia*-derived extracellular vesicles (MCEVs), Anti-oxidation, Anti-inflammation, Microbiota

Introduction

Inflammatory bowel disease (IBD) is a chronic, non-specific inflammatory condition affecting the intestinal tract, encompassing ulcerative colitis (UC) and Crohn's disease (CD) [1]. Presently, over 10 million individuals globally are afflicted with IBD, with a notable rise in incidence observed in Asia [2]. UC is characterized by mucosal inflammation of the colon and can result in ulceration, bleeding, abdominal pain, diarrhea, and other symptoms [3, 4]. Pathologically, mitochondria experience the production and accumulation of ROS. Meanwhile, a reduction system keeps the cells in redox homeostasis [5]. However, the inflammatory response typically promotes the generation of ROS, which in turn amplifies the inflammatory response and triggers the release of inflammatory mediators such as IL-1β, IL-6, TNF-α, and IFN-γ, leading to a self-perpetuating cycle. Elevated levels of ROS and inflammatory factors contribute to the degradation of proteins, lipids, and DNA, ultimately contributing to the pathogenesis of UC [6]. Hence, the regulation of the immune response and the scavenging of excessive ROS are crucial strategies for mitigating UC. The intestinal microbiota is essential for modulating colon immune responses and enhancing intestinal barrier function by producing short-chain fatty acids, bile acids, and multiple bioactive molecules. Therefore, the manipulation of intestinal microbiota also represents a promising treatment option for UC management [7]. Clinically, treatment options for IBD encompass non-targeted therapies, such as aminosalicylic acid, glucocorticoids, and immunomodulators, as well as targeted therapies, like anti-TNF, anti-IL-12/IL-23, and anti-α4β7 integrins. These options are associated with more pronounced side effects, and up to 50% of patients may lose the treatment's effectiveness over time. The emergence of nanomedicines has sparked increased interest in their potential application for treating IBD. Nevertheless, numerous nanomedicines face challenges, including restricted degradation, insufficient biocompatibility, and inefficiencies in loading and releasing external molecules [8]. Consequently, the imperative development of safe and efficacious multi-targeted therapeutic nanomedicines tailored to the pathological features of UC holds significant importance in the prevention and management of UC.

Extracellular vesicles (EVs) are diverse phospholipid bilayer-enclosed entities that modulate intercellular communication by transporting molecular cargo and engaging in surface signaling. EVs are ubiquitously released by various cell types, including plant cells, and are important to facilitate the horizontal transfer of bioactive components such as proteins and nucleic acids (DNA, mRNA, and microRNA), along with other molecules like carbohydrates and secondary metabolites [9, 10]. Recent research has demonstrated the therapeutic

efficacy of plant-derived extracellular vesicles (PDEVs) in treating various diseases, highlighting their safety and yield advantages over mammalian-derived extracellular vesicles and synthetic nanotherapeutics [11]. PDEVs can be readily isolated from a variety of freshly squeezed fruit and vegetable juices, exhibiting pharmacological properties akin to those of the parent plant [12]. Unexpectedly, PDEVs exhibit remarkable stability and resilience in the challenging gastrointestinal milieu, enabling their successful transit to the colon following oral administration. This suggests that PDEVs hold significant promise as effective oral drug delivery vehicles for managing UC.

Momordica charantia, a plant of the genus Momordica in the family Cucurbitaceae, is an annual climber known for its rich content of vitamins, protein polypeptides, saponins, polysaccharides, and other bioactive compounds, earning it the title of "medicinal vegetable". Research has demonstrated that *Momordica charantia* contains quinine and various alkaloids that exhibit diuretic, anti-inflammatory, antipyretic, and ocular benefits [13]. *Momordica charantia* has been shown to enhance the body's immune defense mechanisms. Extracts of *Momordica charantia* exhibit antibacterial and anti-inflammatory properties, particularly against bacteria with notable inhibitory effects. Furthermore, it has been demonstrated that *Momordica charantia* contains antioxidants, intestinal flora regulating, analgesic, and antitumor activities [14]. The extracellular vesicles derived from *Momordica charantia*, known as MCEVs, have been shown to possess the pharmacological properties of the original plant. These properties include the ability to inhibit the growth and spread of brain gliomas [15], prevent cerebral ischemic stroke [16], provide therapeutic benefits in breast and oral cancer cases [17, 18], and protect cardiac myocytes from radiation-induced damage [19]. However, the pharmacological substance basis of MCEVs, the biological mechanism of the antioxidant effects of MCEVs, and the therapeutic effects and biological mechanism of MCEVs on acute UC have still not been revealed.

In this study, high-purity MCEVs with good dispersion were extracted using differential centrifugation and density gradient centrifugation and were comprehensively characterized (Fig. 1). In vitro, we evaluated their anti-inflammatory and antioxidant effects and explored the material basis of their function. In addition, transcriptomics analysis was used to investigate the mechanisms underlying their antioxidant effects. In vivo, we evaluated the biodistribution, the therapeutic and protective effects, and the biological mechanism of orally administered MCEVs in dextran sulfate sodium (DSS) - induced colitis. The study demonstrated that MCEVs had excellent therapeutic effects on UC, significantly restoring the physical and mucosal barriers of the intestinal tract. Mechanistically, this was achieved by reducing intestinal inflammatory cell infiltration, inflammatory factor release, and ROS production. Meanwhile, MCEVs enhance the diversity of the gut microbiota and may restore the intestinal barrier by modulating intestinal indole-related metabolites. Furthermore, proteins, RNA, and other substances in MCEVs contribute to their pharmacological activity. Better retention of MCEVs in the inflamed colon helped them fulfill their therapeutic effects. Our study introduced a novel intervention strategy for ulcerative colitis and investigated the biological mechanisms and material basis of MCEVs in anti-inflammation and antioxidant effects in depth.

Materials and methods

Materials

Lipopolysaccharide (LPS) (from Escherichia coliO55:B5) was purchased from Sigma-Aldrich Corporation (St. Louis, MO, USA). ABScript III RT master mix for qPCR (RK20428), 2X universal SYBR green fast qPCR Mix (RK21203), Bcl-2 Rabbit mAb (A19693), Bax Rabbit mAb (A19684), and β-Actin Rabbit mAb (AC038) were purchased from ABclonal Biotech Co., Ltd (Wuhan, China). The Annexin V-FITC/PI apoptosis assay kit was purchased from Yeasen Biotechnology Co., Ltd (Shanghai, China). DSS was purchased from MP Biomedicals (Santa Ana, CA, USA). Claudin 1 Polyclonal antibody (13050-1-AP), ZO-1 Polyclonal antibody (CL488-21773), Occludin Polyclonal antibody (CL594-13409), CD86 (13395-1-AP), Protein Quantification Kit (BCA Assay) was purchased from Abbkine Scientific Co., Ltd (Wuhan, China).

Isolation and characterization of MCEVs

Momordica charantia L. (family: Cucurbitaceae, genus Momordica, species *Momordica charantia L.*) was purchased from a local supermarket. *Momordica charantia* was rinsed with tap water. The pith was removed, and pulps were cut and juiced. The juice was centrifuged at 3000 g for 30 min and at 10,000 g for 40 min to remove fibers and cellular debris. The post-supernatant was centrifuged at 150,000 g for 90 min, and the precipitated pellet was suspended in PBS. To purify the MCEVs, the suspension was transferred to a discontinuous sucrose gradient (8%, 30%, and 45%) and ultracentrifuged for 2 h at 150,000 g with Optima XE-90 (Indianapolis, U.S.). Bands between 30 and 45% were harvested for MCEVs. The bands were added with PBS and centrifuged at 150,000 g for 2 h to wash away excess sucrose. Finally, the centrifugal precipitate was resuspended in PBS to obtain the final pure product. The protein concentration of MCEVs was assayed using the BCA protein quantification kit. The quantified MCEVs were stored at -80 °C for backup.

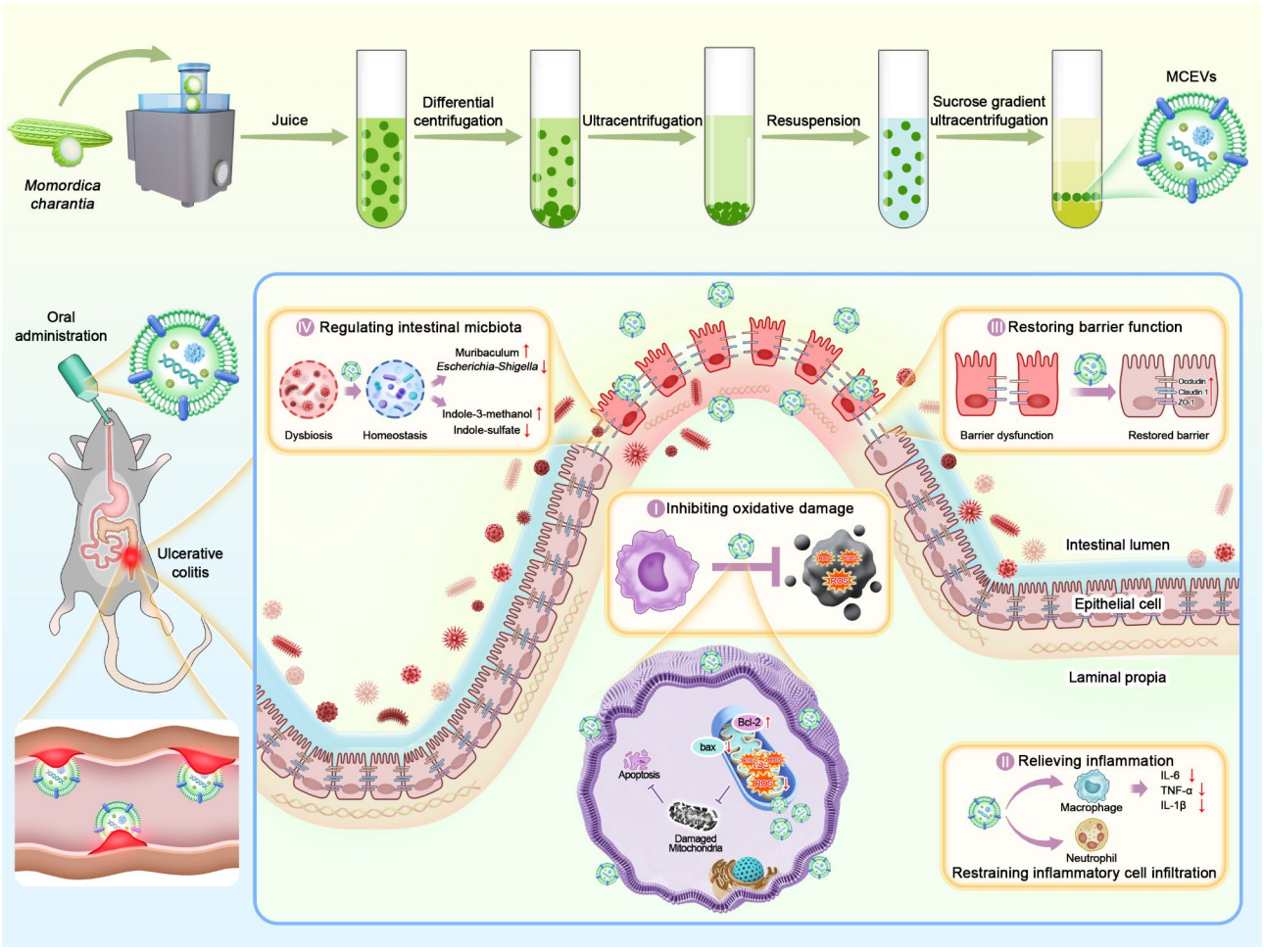

Fig. 1 Schematic illustration of oral administration of MCEVs to alleviate UC by comprehensive renovation of the intestinal microenvironment. **(A)** Preparation of MCEVs by differential centrifugation and density gradient centrifugation. **(B)** Oral administration of MCEVs to comprehensively recover the intestinal damage by inhibiting oxidative damage, relieving inflammation, restoring intestinal barrier function, and regulating intestinal flora to alleviate UC

For TEM imaging, a drop of sample was deposited on the surface of formvar-coated copper grids, followed by the addition of 2% phosphotungstic acid negative staining solution for 2 min, and then the sample was dried at room temperature for subsequent imaging. The size and zeta potential of MCEVs were analyzed with the Malvern Zetasizer Nano ZS90 instrument (WorcesterShire, UK).

Component analysis of MCEVs

MCEVs were submitted to the Hangzhou Lianchuan Biology Institute (Hangzhou, China) for lipidomic, proteomic, and microRNA sequencing analysis. Lipidomics and metabolites are extracted using the organic reagent precipitation metabolite method. The samples were detected by mass spectrum scanning. MetaX software was used for metabolite identification, and the identified metabolites were annotated in the database of common functions, and then the metabolites were quantitatively analyzed. Proteomic: the proteins were extracted and assessed, and the quality-checked protein samples were subjected to Trypsin degradation separately. Each sample was subjected to nano-HPLC reversed-phase chromatographic separation and mass spectrometric detection, respectively. Protein identification and LFQ quantification were carried out using PD/MaxQuant library software. MicroRNA sequencing: The sRNA sequencing library preparation was performed first. The constructed libraries were sequenced using Illumina HiSeq 2000/2500 with a single-end 50 bp read length (SE50). MCEVs were submitted to Suzhou PANOMIX Biomedical Tech Company for untargeted metabolomics analysis. In brief, thaw the experimental sample at 4℃ and mix it evenly after thawing. Filter the supernatant through a 0.22 μm membrane following centrifugation, then transfer it to a detection bottle for LC-MS analysis.

In vitro antioxidant ability of MCEVs

ABTS assay: ABTS + radicals were first prepared by mixing ABTS- (7 mM) with potassium persulfate (K2S2O8, 2.45 mM) at room temperature for 12 h. The

corresponding concentrations (1, 2.5, 5, 10, and 20 μg/mL) of MCEVs were taken and incubated with ABTS+, and the absorbance at 734 nm was recorded by zymography (TECAN, Switzerland).

DPPH assay: 75 μM DPPH was mixed with an equal volume of ethanol. Then 10 μL MCEVs were added for 30 min making the final concentration of MCEVs 25, 50, 100, 150, and 300 μg/mL. The absorbance was measured at 517 nm by zymography (TECAN, Switzerland). UV absorption at 490–580 was detected by a UV-Vis spectrophotometer.

TMB assay: 10 μL FeSO4 (100 μM), 10 μL H_2O_2 (500 μM), 10 μL TMB (3mM) and 60 μL H_2O were added together. Then 10 μL MCEVs were added, making the final concentration of MCEVs 10, 20, 40, 60, and 80 μg/mL. The absorbance was measured at 645 nm by zymography (TECAN, Switzerland). UV absorption at 530–760 was detected by a UV-Vis spectrophotometer.

EPR assay: Electron paramagnetic resonance (EPR) spectrometer was used to characterize radicals in the reaction system. EPR spectra were measured on CIQTEK EPR200M manufactured by CIQTEK Co., Ltd. (Hefei, China).

Cell culture

RAW 264.7 macrophage cells and normal human fetal colonic epithelial cells (HFC) were obtained from the American Type Culture Collection (ATCC, USA), cultured in DMEM high glucose medium.

Cellular uptake and biodistribution assays

Synthesis of DiL/DiR-MCEVs: MCEVs were labeled with the lipophilic fluorescent dye DiL or DiR by incubating a 10 mM solution of the dye with 1 mg of MCEVs. The labeled MCEVs were subsequently purified by passing them through a 100 kDa ultrafiltration device to remove any unbound dye molecules.

DiL-labeled MCEVs were added to RAW 264.7 cells to co-incubate for 4, 8, and 12 h. Then, cells were washed 3 times with PBS to clear spared DiL-labeled MCEVs. Flow cytometry was used to detect the DiL-positive cells. A fluorescence microscope was used to capture the real cellular uptake pictures. Before that, cells should be fixed with 4% paraformaldehyde. After washing cells 3 times, the F-actin of cells was stained with green FITC-Phalloidin, and the nuclei of cells were stained with blue DAPI. Then, cells could be imaged by Carl Zeiss Microscopy Axioscope 5 (Oberkochen, Germany).

After 12 h of fasting, mice were gavaged with 100 μL DiR-labeled MCEVs and imaged in vivo at 1, 6, 12, and 24 h. At each time point, the hearts, livers, spleens, lungs, kidneys, and gastrointestinal tracts of the mice were collected and imaged using the VISQUE Invivo Smart-LF system (Montreal, Canada).

Cellular antioxidant effects of MCEVs

MCEVs (5 μg/mL and 10 μg/mL) were co-incubated with RAW 264.7 macrophage cells for 12 h. Then, H_2O_2 (400 μM) was co-incubated for another 4 h to induce ROS production. After that, the DCFH-DA probe was diluted to 10 μM by PBS and stained cells for 1 h. DCF-positive cells were detected by flow cytometry.

RAW 264.7 macrophage cells were plated in 96-well plates at a density of 50–60% and co-incubated with MCEVs (5 μg/mL and 10 μg/mL) for 12 h. Then, 5 μL H_2O_2 was added for 6 h, making the H_2O_2 final concentration 0.5 mM, 0.8 mM, and 1.0 mM. Cell viability was then assessed using the MTT assay.

RNA sequencing of cells

MCEVs (10 μg/mL) were applied to RAW 264.7 macrophage cells for incubation. Subsequently, H2O2 (800 μM) was co-incubated for an additional 6 h. Cells were collected using RNA protect reagents. The collected samples were sent to LC-Bio Technologies Co., Ltd (Hangzhou, China) for RNA sequencing analysis. The experimental steps are as follows:

Total RNA was isolated using TRIzol reagent, with purity and integrity verified by NanoDrop (RIN > 7.0) and Bioanalyzer. Poly(A) RNA was enriched using magnetic beads, fragmented, and reverse-transcribed into double-stranded cDNA. After A-tailing and ligation to indexed adapters, library fragments were size-selected with AMPureXP beads. UDG enzyme treatment removed U-labeled second-strand DNA, followed by PCR amplification to construct libraries (average insert size: 300 ± 50 bp). Sequencing was performed on the Illumina NovaSeq 6000 platform (PE150). Raw data were quality-filtered using Fastp, aligned to the human genome (GRCh38) via HISAT2, and assembled with StringTie to calculate FPKM values. Differentially expressed mRNAs were identified using edgeR ($p < 0.05$).

Cellular anti-inflammatory effects of MCEVs

MCEVs (10 μg/mL) were applied to RAW 264.7 macrophage cells for incubation. Then, LPS (500 ng/mL) was co-incubated for another 12 h to induce inflammatory factor expression. Then, total RNA was extracted by a total RNA extraction kit. Ultimately, qRT-PCR assay was used to assess inflammatory factor expression.

Cellular mitochondrial damage and apoptosis

MCEVs (10 μg/mL) were applied to RAW 264.7 macrophage cells for incubation. Then, H_2O_2 (600 μM) was co-incubated for another 5 h, and H_2O_2 (800 μM) was co-incubated for another 6 h to induce cell mitochondrial damage and cell apoptosis separately. After co-incubation with a JC-1 probe for 1 h, flow cytometry and a microscope were used to detect mitochondrial damage. After

co-incubation with Annexin V-FITC/PI dye, flow cytometry was used to detect cell apoptosis.

Western blotting analysis

MCEVs (10 μg/mL) were added to RAW 264.7 macrophage cells seeded in 6-well plates and incubated for 12 h. H_2O_2 (800 μM) was co-incubated for another 6 h to induce cell apoptosis. Cells were lysed by mixing RIPA cell lysate and protease inhibitor. BCA protein quantification kit measured protein concentration. 50 μg protein was mixed in the loading buffer and then heated at 95℃ for 10 min, making protein denaturation. After loading 20 μL of protein samples, a 5% stacking gel was run at 80 V, and a 10% separating gel was run at 110 V using the Mini-PROTEAN® Tetra Vertical Electrophoresis system (California, USA). Next, proteins on the gel were transferred to the PVDF membrane. The primary antibody was diluted 1:1000. The β-actin was diluted 1:10000. After washing with TBST buffer, the membrane was co-incubated with the primary antibody for 12 h at 4℃. The membrane was washed 3 times with TBST and was incubated with HRP-conjugated goat anti-rabbit IgG. Finally, the protein bands were exposed using a gel imaging system after reacting with ECL solution.

Quantitative real-time PCR (qRT-PCR)

1 μg RNA was mixed with 4 μL ABScript III RT master mix and DEPC water to a final volume of 20 μL. RNA was transcribed to cDNA following the manufacturer's recommended procedure. The cDNA template was diluted tenfold and mixed with 10 uL 2X universal SYBR Green Fast qPCR Mix, 2 μL primer, and 3 μL DEPC water. According to the instructions, inflammatory factor expression was measured using the Real-time fluorescent quantitative PCR System (Hangzhou, China). The primer sequences are shown in Table S2.

Immunofluorescence analysis

Colonic tissues were cryosectioned to analyze the expression of tight junction proteins. Sections were flushed three times with PBS and then were incubated with 0.2% Triton X-100 for 8 min. Then the sections were flushed with PBS. Block non-specific proteins with 1% BSA. Incubate overnight with primary antibody (dilution 1:100) at 4 °C. After washing, slides were blocked with DAPI and visualized by fluorescence microscopy.

Animals

C57BL/6 mice (6–8 weeks old) were purchased from the Medical Laboratory Animal Center of Xi'an Jiaotong University, Shaanxi Province, China. All animal experiments were performed and approved by the Xi'an Jiaotong University Laboratory Animal Care Committee, according to the Principles of Laboratory Animal Care and Guidelines.

Biocompatibility and biosafety evaluation

RAW 264.7 macrophage cells were co-incubated with different concentrations of MCEVs (0.5, 1, 5, 10, 20, 30, 40, and 50 μg/mL) for 12 and 24 h. The relative survival of RAW 264.7 cells was determined using the standard MTT assay.

Mice were gavaged 30 mg/kg MCEVs for 7 consecutive days, and after waiting for one day, the mice were sacrificed, and blood was taken from the eyeballs. A part of the blood was used for routine blood tests, and another part was centrifuged to collect serum for blood biochemistry analysis using Hemo 3600 V hematology analyzer (Shanghai, China). Meanwhile, internal organs were isolated and fixed with 4% PFA for over 24 h for H&E staining.

HE staining and Alcian blue staining

Colon tissue was gradient dehydrated and then paraffin-embedded. Colon paraffin blocks were cut into 7 μm slices. Slices were immersed in xylene for 20 min to remove waxes, followed by immersion in 95%, 85%, 75%, and 50% graded alcohols to wash away xylene, and hematoxylin staining for cell nuclei for 4 min continuously. Then, the slices were soaked in distilled water for 10 min, immersed in 50%, 70%, and 85% graded alcohol for 3 min, and stained with eosin solution for 30 s. Thereafter, anhydrous ethanol was used to wash off the excess dye, and slices were immersed in xylene for 20 min. Meanwhile, mucin was stained according to Alcian Blue staining kit instructions. Finally, microscopic observation was carried out after resin sealing.

Analysis of intestinal contents flora and metabolomics

The intestinal contents of therapeutic modeling mice were collected. Liquid nitrogen is treated and stored at -80℃. The samples were then sent to LC-Bio Technologies Co., Ltd (Hangzhou, China) for bacterial 16srDNA sequence sequencing and non-targeted metabolomics analysis. The experimental steps are as follows:

Fecal microbial DNA was extracted, and the V3-V4 regions were amplified using universal primers 341 F/805R. Purified PCR products were sequenced on the Illumina NovaSeq 6000 platform (PE250). Raw data underwent adapter removal, quality filtering, and chimera elimination. ASVs were generated using DADA2, followed by taxonomic annotation against the SILVA/NT-16 S databases. Alpha/beta diversity analyses were performed with QIIME2. Differentially abundant genera were identified via the Wilcoxon rank-sum test ($P < 0.05$) and LEfSe (LDA ≥ 3.0, $P < 0.05$), with visualizations generated using R packages.

Statistical analysis

All results were statistically analyzed using Student's t-test and shown as mean ± standard deviation (SD). $^{*}P < 0.05$, $^{**}P < 0.01$, $^{***}P < 0.001$ indicate statistical differences, and ns is not statistically significant.

Results

Extraction and characterization of MCEVs

The crude extract product was acquired through differential centrifugation following the extraction of *Momordica charantia* juice. Subsequently, it was purified via density gradient centrifugation, resulting in MCEVs primarily within the 30–45% range. Transmission electron microscopy (TEM) results revealed that the MCEVs displayed a spherical morphology of approximately 200 nm, had an intact membrane structure, and were consistent with the structural features of the extracellular vesicle (Fig. 2A) [20]. Dynamic light scattering (DLS) results indicated that the hydrodynamic particle size of the MCEVs was 164.3 ± 68.16 nm, with a polydispersity index (PDI) averaging approximately 0.212 (Fig. 2B). Additionally, MCEVs within this size range exhibited a zeta potential of -28.1 ± 3.78 mV (Fig. 2C). To further assess the stability of MCEVs, we incubated them with

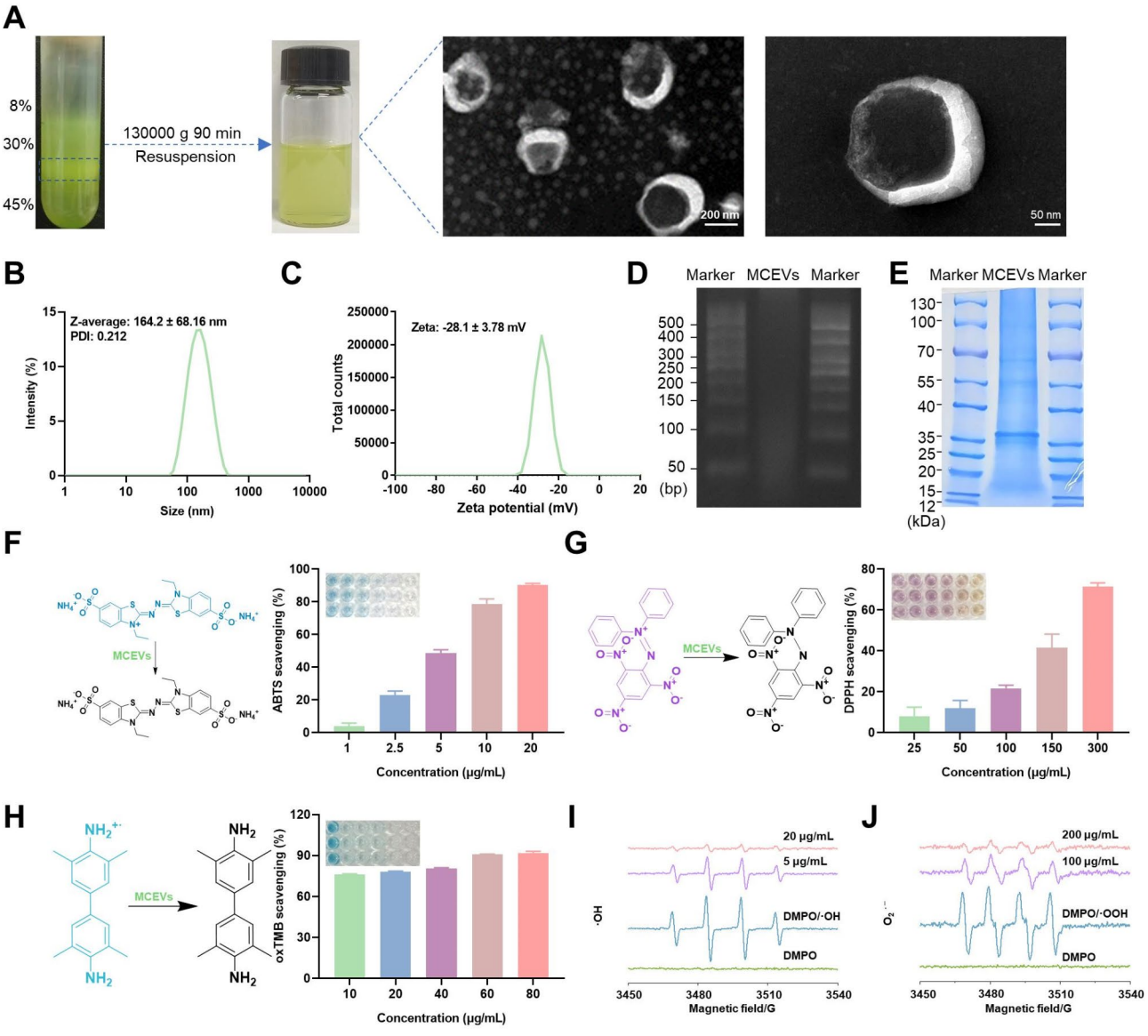

Fig. 2 Characterization of MCEVs. **(A)** Picture after sucrose gradient ultracentrifugation and TEM images of MCEVs. **(B)** Hydrated particle size of MCEVs. **(C)** Zeta potential of MCEVs. **(D)** Agarose gel electrophoresis of MCEVs. **(E)** Protein gel electrophoresis of MCEVs. **(F)** Total antioxidant capacity test of MCEVs by the ABTS radical scavenging ($n = 3$). **(G)** DPPH radical scavenging capacity test of MCEVs and schematic illustration of DPPH radical scavenging. **(H)** •OH scavenging capacity test of MCEVs and schematic illustration of oxTMB reaction ($n = 3$). **(I)** ESR spectra indicating the •OH scavenging capacity of MCEVs. **(J)** ESR spectra indicating $O_2^{\bullet-}$ scavenging capacity of MCEVs. Data were shown as mean ± SD

NaCl, culture medium and serum at 37 °C for 30 min. The particle size of MCEVs in NaCl and culture medium did not change significantly (Fig. S1A and B), and the MCEVs in serum remained intact under TEM (Fig. S1C). Agarose gel electrophoresis results showed the presence of nucleic acids in the MCEVs (Fig. 2D). Sodium dodecyl sulfate polyacrylamide gel electrophoresis (SDS-PAGE) results revealed a broad distribution of protein molecular weights within the range of 15–100 kDa (Fig. 2E). These results demonstrated that we successfully extracted MCEVs with uniform particle size, good dispersion, enriched contents and high purity.

Since *Momordica charantia* is generally considered to have antioxidant effects, a comprehensive evaluation of its antioxidant capacity and effectiveness in scavenging reactive nitrogen species was initially conducted in vitro. The evaluation included assays for ABTS radical, DPPH radical, and reactive oxygen species (ROS), such as hydroxyl radicals (•OH) and superoxide anions ($O_2^{\bullet-}$). The ABTS radical scavenging assay, a method used to indirectly measure the antioxidant capacity of a substance, indicated that lower concentrations of MCEVs were able to neutralize more than 80% of free radicals (Fig. 2F). The DPPH free radical scavenging experiment, which assesses the ability to neutralize nitrogen-centered radicals, showed that MCEVs at a concentration of 300 μg/mL exhibited a scavenging capability of more than 60% for the DPPH radical (Fig. 2G). Additionally, the oxidation of TMB (3,3′,5,5′-tetramethylbenzidine) to oxTMB by hydroxyl radicals (•OH) was used as an indicator of oxidative reactions. Experimental data revealed that a lower concentration of MCEVs (10 μg/mL) could inhibit over 60% of TMB oxidation (Fig. 2H). These results were further confirmed using UV spectrophotometry (Fig. S1D and E). A bench-top Electron Paramagnetic Resonance (EPR) Spectrometer was employed to quantify free radicals by analyzing the EPR spectra of adducts formed following the interaction of free radicals with a trapping agent. The findings demonstrated that MCEVs (20 μg/mL) exhibited notable scavenging activity against •OH and resulted in a marked decrease in $O_2^{\bullet-}$ in the incubation group upon the introduction of MCEVs (Fig. 2I, J). Taken together, these investigations suggested that MCEVs possessed remarkable antioxidative capacity and have potential for use in treating or preventing diseases associated with oxidative stress.

The intracellular uptake and anti-inflammatory effects of MCEVs

The internalization of PDEVs facilitates the transportation of enclosed compounds, thereby enabling PDEVs to perform a function within cellular environments [21]. To further explore the cellular internalization and impact of MCEVs, we used the RAW 264.7 macrophage cell line as a model to assess their anti-inflammatory potential. RAW 264.7 cells were cultured with DiL-labeled MCEVs for varying durations, and cellular uptake was assessed by fluorescence microscopy and flow cytometry. It was demonstrated that the uptake of MCEVs was time-dependent, with the uptake rate increasing as incubation time progressed. After 12 h of incubation, the uptake rate reached 58.4%. (Figs. 3A, B, and S2). Macrophages, when stimulated by pathogen-associated molecular patterns, typically differentiate into M1 pro-inflammatory subtypes. These cells release pro-inflammatory cytokines, induce ROS production, and recruit other inflammatory cells, thereby accelerating intestinal barrier damage and exacerbating the UC process [22]. LPS stimulation of RAW 264.7 macrophages can be used to model inflammatory responses in vitro. The levels of inflammatory cytokines (IL-6, IL-1β, and TNF-α) were notably heightened following LPS stimulation. However, when cells were pre-incubated with MCEVs for 12 h before LPS stimulation, this increase was significantly attenuated (Fig. 3C-E). Immunofluorescence staining revealed that pre-incubation with MCEVs significantly suppressed LPS-induced overexpression of the M1 subtypes marker CD86 (Fig. 3F). Moreover, ROS probe (DCFH-DA) and flow cytometry assays showed that LPS-induced inflammatory response was accompanied by an increase in ROS levels, which were remarkably inhibited by MCEVs (Fig. 3G, H). These results indicated that MCEVs could not only inhibit the inflammatory response but also alleviate the oxidative stress caused by the inflammatory response.

The intracellular antioxidant effects and biological mechanisms of MCEVs

Due to the notable ROS clearance capabilities of MCEVs observed in vitro, cellular stimulation with H_2O_2 was employed to model oxidative stress. Flow cytometry analysis revealed that the group stimulated with H_2O_2 alone exhibited 58.6% DCF + cells. Conversely, there was a notable decrease in ROS production in cells pre-incubated with 5 μg/mL and 10 μg/mL MCEVs for 12 h before H_2O_2 stimulation (Fig. 4A, B). The overproduction of ROS is known to result in cellular oxidative damage and, ultimately, cell death [23]. MTT assays showed a marked reduction in cell viability as the H_2O_2 concentration increased. Conversely, pre-incubation with varying concentrations of MCEVs for 12 h significantly inhibited H_2O_2-induced cell death, with higher concentrations of MCEVs proving to be more effective in this regard (Fig. 4C). To further elucidate the biological mechanisms underlying the antioxidant activity of MCEVs, transcriptomic analysis was conducted on cells subjected to various treatments, including an untreated negative control group (Control), a group stimulated with H_2O_2 alone (H_2O_2), and a group treated with 10 μg/mL

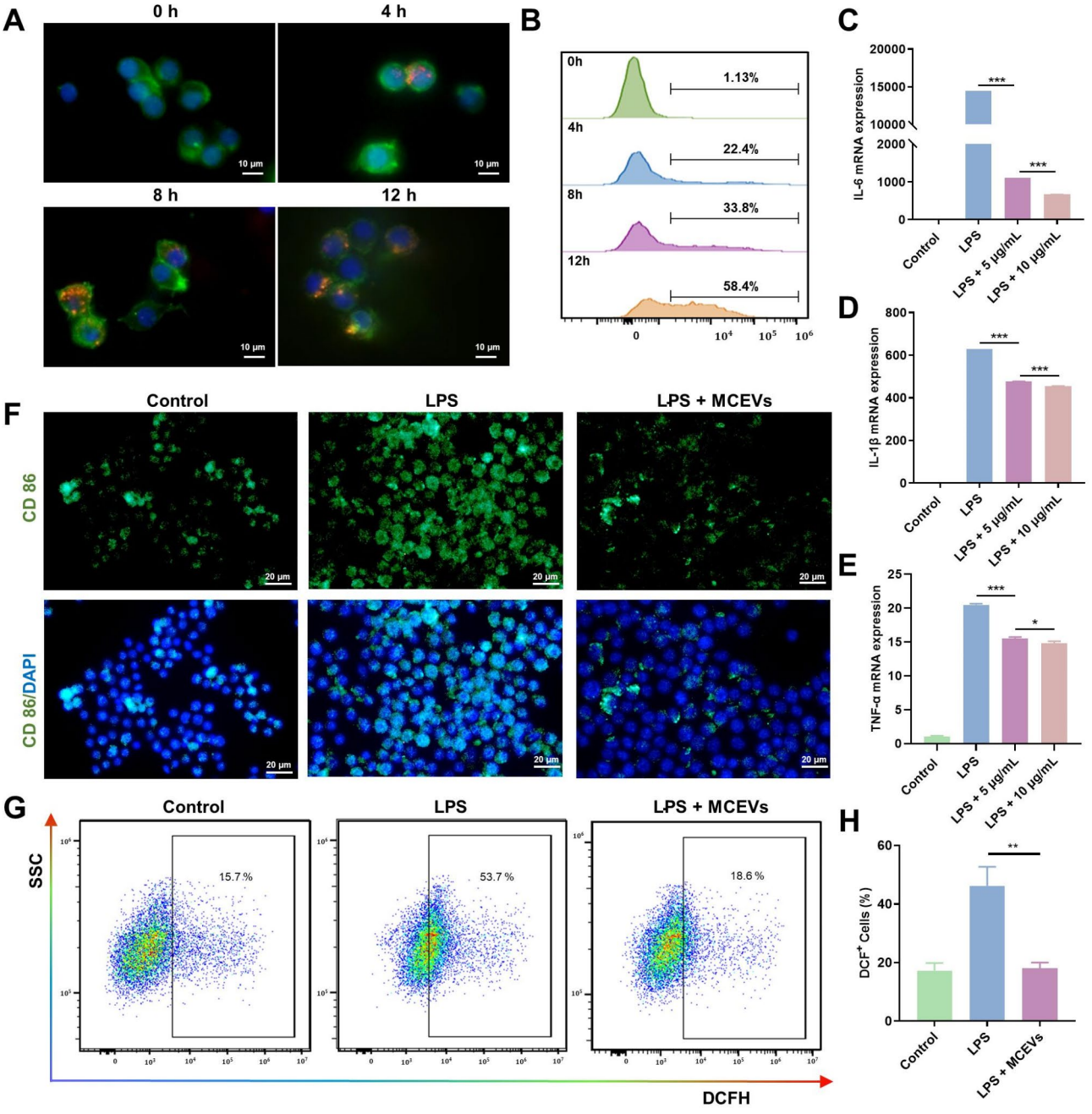

Fig. 3 The intracellular uptake and anti-inflammatory effects of MCEVs. **(A)** Fluorescent staining to show cellular uptake of MCEVs after 4, 8, and 12 h. MCEVs were labeled with red DiL dye. The cytoskeleton was stained with green FITC-Phalloidin dye. The nucleus was stained with blue DAPI dye. **(B)** A representative image of the cellular uptake efficiency of MCEVs shown by flow cytometry. **(C-E)** qRT-PCR to evaluate the transcription level of inflammatory cytokines by RAW 264.7 cells after incubation with MCEVs for 12 h and then 500 ng/mL LPS induced for 12 h. **(F-H)** RAW 264.7 cells were incubated with 10 μg/mL MCEVs for 12 h and then induced by 500 ng/mL LPS for 12 h. **(F)** Representative images of CD86 antibody immunofluorescence staining of M1 macrophages. **(G)** Flow cytometry was used to detect the level of ROS by DCFH-DA ROS probe. **(H)** Statistical map of DCF-positive cells. Data were shown as mean ± SD. $n \geq 3$, *: $P < 0.05$, **: $P < 0.01$, ***: $P < 0.001$, ns: $P > 0.05$, indicating no significance

for 12 h before H_2O_2 stimulation (H_2O_2 + MCEVs). The transcriptomic differential gene enrichment heatmap revealed a substantial number of differentially expressed genes (Fig. 4D). Volcano plot analysis revealed that the H_2O_2 + MCEVs group exhibited significant up-regulation of 528 genes and down-regulation of 360 genes compared with the H_2O_2 group (Fig. 4E). Additionally, the differential genes in these two groups were found to be enriched in cellular components such as the mitochondrial membrane and mitochondrial respiratory chain (Fig. 4F). Subsequently, the genes associated with mitochondria and apoptosis were notably altered following stimulation with

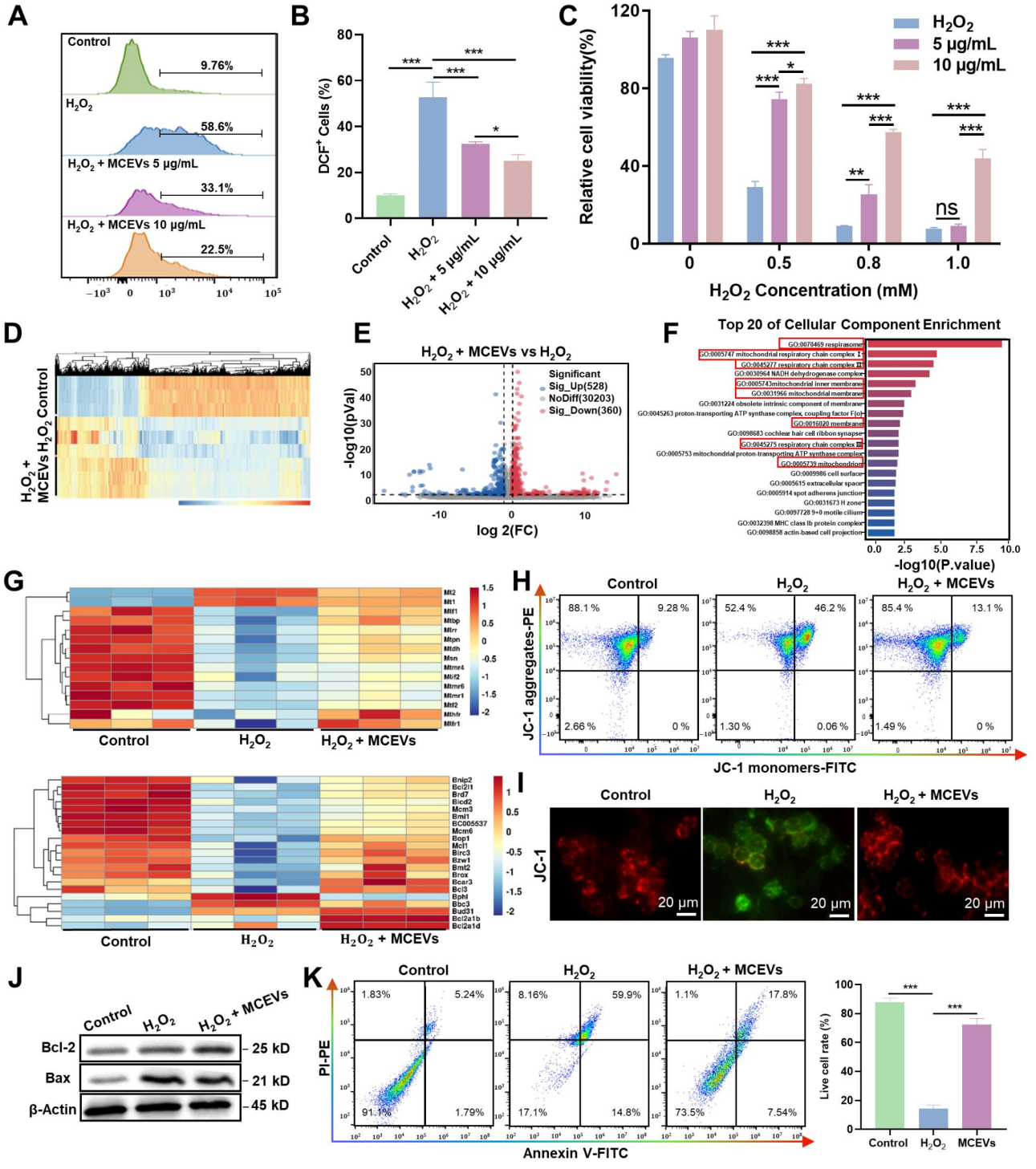

Fig. 4 The intracellular antioxidant effects and biological mechanisms of MCEVs. **(A-B)** Flow cytometry was used to detect the level of ROS by DCFH-DA ROS probe after the MCEVs treatments. **(C)** The cell activity after being co-incubated with MCEVs was affected by different concentrations of H_2O_2. **(D)** Heatmap cluster analysis for the total RNA-seq genes of the control group, H_2O_2 group, and H_2O_2 + MCEVs group. **(E)** Volcano plots of upregulated genes (in red) and downregulated genes (in blue) of the H_2O_2 + MCEVs group compared to the H_2O_2 group (p-value < 0.05 and fold change (FC) > 1.5). **(F)** Top 20 cellular component enrichment analysis after MCEVs treatment compared to the H_2O_2 group. **(G)** Heatmap plot of mitochondria-related and apoptosis-related genes of the control group, H_2O_2 group, and H_2O_2 + MCEVs group. **(H)** Flow cytometry was used to assess MMP under the MCEVs treatment by the JC-1 probe. **(I)** Fluorescence microscopy imaging was employed to evaluate MMP following treatment with MCEVs using the JC-1 probe. **(J)** Western blotting analysis of the protein levels of Bcl-2 and Bax. **(K)** Apoptosis of RAW 264.7 macrophage cells was assessed by flow cytometry with Annexin V-FITC/PI staining. Data were shown as mean ± SD. $n \geq 3$, *: $P < 0.05$, **: $P < 0.01$, ***: $P < 0.001$, ns: $P > 0.05$, indicating no significance

H_2O_2. Unexpectedly, treatment with MCEVs was found to attenuate this observed trend. Furthermore, there was a considerable increase in the transcription of anti-apoptotic proteins, such as Bcl2a1b and Bcl2a1d (Fig. 4G).

ROS activate multiple pathways of apoptosis, including those involving mitochondria, death receptors, and the endoplasmic reticulum. Mitochondria-dependent apoptosis is a well-known mechanism of programmed cell death, wherein cellular stress or apoptotic signals can result in the release of cytochrome c from the mitochondria. This released cytochrome c acts as an apoptosis inducer by forming a complex with Apaf-1, the precursor of caspase-9, and ATP/dATP, ultimately activating caspase-3. The Bcl-2 protein family is vital in controlling apoptosis by influencing mitochondrial permeability [24–26]. Combined with the transcriptomic results, it was hypothesized that MCEVs alleviated mitochondrial oxidative damage by scavenging ROS, protecting mitochondrial structures and functions, regulating apoptosis-related proteins, and inhibiting mitochondria-dependent apoptosis.

To confirm this hypothesis, a JC-1 probe was employed to evaluate alterations in mitochondrial membrane potential (MMP). Consistent with expectations, the presence of intracellular JC-1 monomers markedly increased following H_2O_2 stimulation, while pre-incubation with MCEVs led to a reduction in JC-1 monomers (Fig. 4H). Additionally, fluorescence microscopy images supported these findings, indicating that MCEVs effectively attenuated the H_2O_2-induced alterations in MMP (Fig. 4I). Western blotting analysis revealed that MCEVs significantly reversed the overexpression of the pro-apoptotic protein Bax, along with the reduced expression of the anti-apoptotic protein Bcl-2 induced by H_2O_2 (Fig. 4J). The utilization of Annexin V in conjunction with a FITC fluorescent probe enabled the identification of early apoptotic cells, while the use of PI staining solution facilitated the detection of late apoptotic and necrotic cells. Through the integration of flow cytometry, we confirmed that MCEVs effectively suppressed H_2O_2-induced apoptosis, as shown in Fig. 4K. Overall, our findings support the hypothesis that MCEVs may mitigate mitochondria-dependent apoptosis by preserving the integrity of mitochondrial membranes and regulating apoptosis-related proteins.

The material basis for the role of MCEVs

The plant-derived EVs were found to harbor a broad range of proteins, nucleic acids, and small molecule compounds originating from the parent cells [27]. To explore the material basis for the functioning of MCEVs, a comprehensive analysis of their chemical composition was conducted. Specific protein species were identified using liquid chromatography-tandem mass spectrometry (LC-MS/MS). The total ion chromatogram revealed the identification of 418 proteins (Table S2). Bioinformatics analysis indicated that over 80% of these proteins were associated with metabolic processes, such as amino acid and carbohydrate metabolism (Fig. 5A). Additionally, 226 miRNAs ranging in length from 18 to 25 nucleotides were detected in MCEVs (Fig. 5B and Table S3). Non-targeted metabolomics and lipidomics analyses identified 320 metabolites and 667 lipids, respectively (Tables S4 and S5). Among the metabolites, the predominant compound classes included organic oxygenates (43.81%), carboxylic acids and their derivatives (19.97%), and fatty acids (8.96%) (Fig. 5C). MCEVs exhibited enrichment in diglycerides (DG, 24.32%), phosphatidylcholine (PC, 10.46%), and acylhexosyl stigmasterol (AHexSTS, 10.35%) (Fig. 5D). Compounds such as β-carotene, lycopene, astaxanthin, and phosphatidylcholine, which are known for their antioxidant properties [28–30], were also identified. Additionally, phosphatidylcholine (PC), known for its anti-inflammatory effects, holds potential for treating inflammatory bowel disease [31]. These results suggested that MCEVs possess good pharmacological activities and have great potential for application in the field of disease treatment.

The above results suggested that MCEVs are abundant in nucleic acids, proteins, lipids, and small molecules. Therefore, it is necessary to explore which categories of molecules are responsible for the pharmacological activity of MCEVs. Based on the previous study [32], RNase or protease was used to remove RNA or protein, respectively, followed by ultrafiltration to remove excess enzyme or enzyme digestion products (Fig. 5E). Agarose gel electrophoresis and polyacrylamide gel electrophoresis confirmed that RNase A successfully digested RNA, and after treatment with Proteinase K, the protein was digested into small peptides below 12 kDa (Fig. 5F, G). TEM images reflected that the structure of MCEVs remained intact after enzyme incubation (Fig. S3). The digestion of RNA or proteins compromised the anti-inflammatory effects of MCEVs, with protein digestion having a greater impact on the inhibitory effects of IL-6 and TNF-α. Although simultaneous removal of protein and RNA had the most significant influence on the anti-inflammatory effects of MCEVs, proteins and RNA digestion MCEVs still retained the ability to inhibit the secretion of inflammatory factors (Fig. 5H). These results suggested that proteins, RNAs, and other materials in MCEVs collectively contributed to their pharmacological activity.

In vivo biocompatibility of MCEVs

High-quality biosafety is crucial for the clinical translation of MCEVs in the medical field. Consequently, a comprehensive assessment of the biosafety of MCEVs

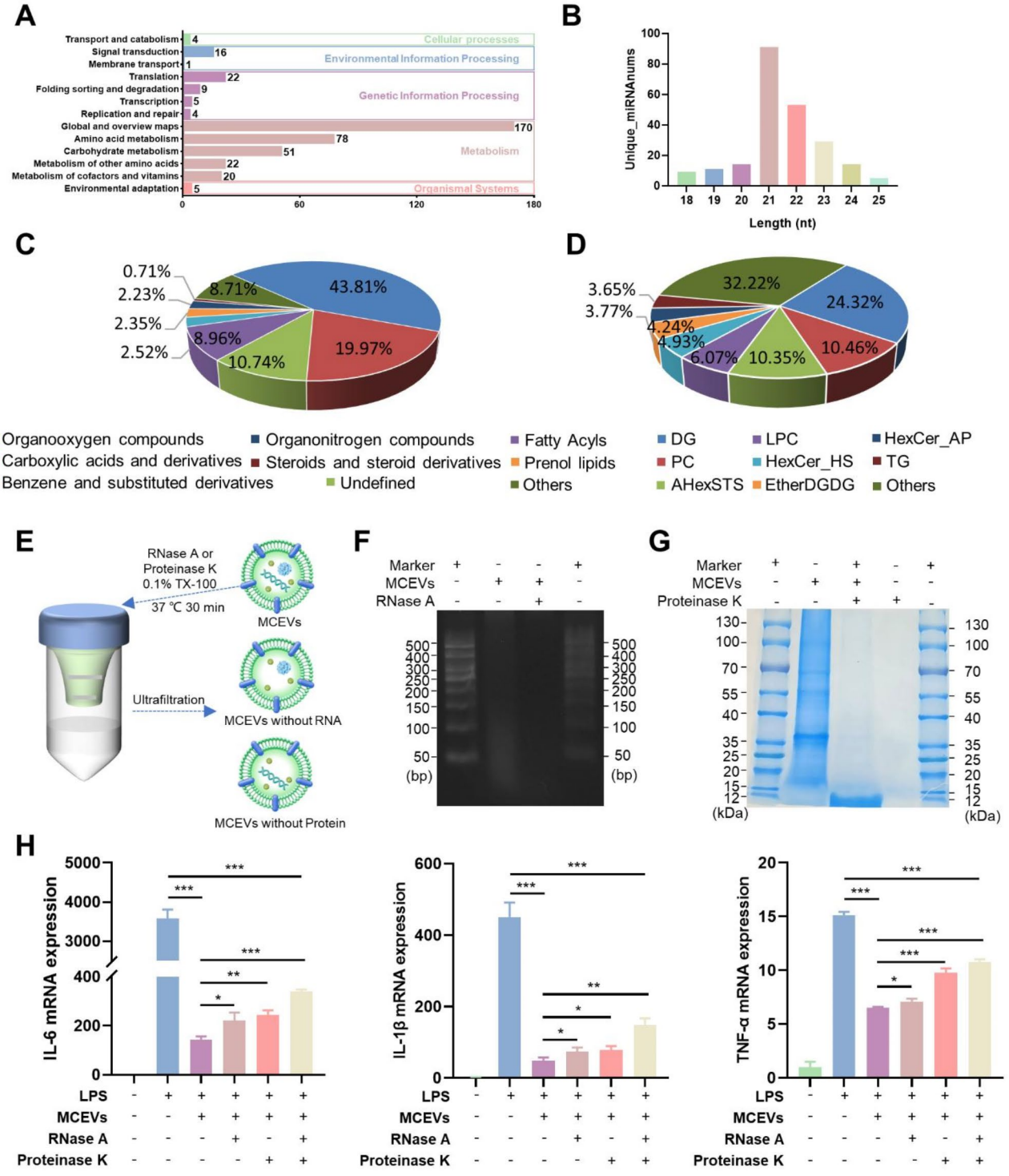

Fig. 5 The material basis of the efficacy of MCEVs. **(A)** KEGG annotated statistical charts of identified proteins in MCEVs. **(B)** Length distribution of miRNAs in MCEVs. **(C)** Relative quantification analysis of metabolites classes in MCEVs. **(D)** Relative quantification analysis of lipid classes in MCEVs. **(E)** Detection of nucleic acids of MCEVs after RNase A treatment by agarose gel electrophoresis. **(F)** Detection of protein of MCEVs after Proteinase K treatment by protein gel electrophoresis. **(G)** Schematic diagram of ultrafiltration method for removing excess impurities after enzymatic digestion. **(H)** qRT-PCR to evaluate the transcription level of inflammatory cytokines by RAW 264.7 macrophage cells after incubation with MCEVs of different treatments for 12 h and then LPS induced for 12 h. Data were shown as mean ± SD. $n \geq 3$, *: $P < 0.05$, **: $P < 0.01$, ***: $P < 0.001$, ns: $P > 0.05$, indicating no significance

was conducted at both the cellular and animal levels. Cell viability was evaluated using the MTT assay after co-incubation with MCEVs at concentrations ranging from 0 to 10 μg/mL for 12 and 24 h in RAW264.7 and FHC cells. Additionally, apoptosis was assessed using flow cytometry following a 24-hour co-incubation in RAW264.7 cells. The findings consistently demonstrated that over 90% of cells remained viable across various treatment conditions, suggesting the biocompatibility of MCEVs with cellular systems (Fig. 6A, B, and D). The biosafety of MCEVs in mice was further assessed through a study in which mice in the MCEVs group were administered 30 mg/kg of MCEVs for 7 consecutive days. Daily monitoring of body weight changes was conducted, and on the 9th day, the mice were euthanized to extract vital organs and blood for analysis. Results indicated no notable difference in body weight between the MCEVs group and the control group (Fig. 6C). Histological assessment of organs was conducted using H&E staining, revealing the absence of histological lesions and cellular damage following treatment with MCEVs (Fig. 6E). Furthermore, analysis of blood routine and biochemical indexes indicated no statistical significance between the MCEVs group and the healthy control group (Fig. 6F, G). These results supported the conclusion that MCEVs exhibited favorable safety profiles following oral administration, warranting further in vivo investigation.

The stability and colonic retention effects of MCEVs

Considering the remarkable anti-inflammatory and antioxidant effects of MCEVs demonstrated in vitro, as well as their good biosafety profile in vivo, we were prompted to explore the biodistribution of MCEVs after oral administration to assess their potential for application in the prevention and treatment of UC. To evaluate the stability of MCEVs after oral administration, MCEVs were incubated in simulated intestinal fluid at 37 °C for 4 h, followed by simulated gastric fluid at 37 °C for another 4 h. TEM images showed that the morphology of MCEVs remained intact (Fig. 7A). Next, we used in vivo imaging technology to examine the distribution of DiR-labeled MCEVs in healthy and DSS-induced UC mice after equal gavage. The findings indicated that DiR-labeled MCEVs were metabolized more rapidly in healthy mice, whereas they were retained longer in UC mice, with residues still present at 24 h (Fig. 7B, E). Fluorescence could be observed in the colon after 1 h of oral administration of DiR-labeled MCEVs, with the strongest fluorescence in the colon at 6 h. The fluorescence intensity then decreased over time and disappeared completely at 24 h in the healthy (Control) group. In contrast, DiR-labeled MCEVs reached the colons of UC mice after 1 h, with the greatest colonic enrichment at 6 h, and remained in the colons of UC mice at 24 h (Fig. 7D, G). During this process, fluorescence was observed only in the gastrointestinal tract and not in any of the organs (heart, liver, spleen, lungs, kidneys) (Fig. 7C, F). These results suggested that MCEVs could cross the gastrointestinal tract to reach the colon and remain in the colon of UC mice for a longer time. This phenomenon reinforced the potential application of MCEVs for UC treatment.

The therapeutic effect of MCEVs on UC

Given the promising anti-inflammation effects observed in vitro and the biocompatibility demonstrated in vivo, our studies aimed to determine whether MCEVs maintain the therapeutic efficacy of *Momordica charantia* in a DSS-induced UC model. Initially, four groups were established: a blank control group, a DSS group, a group receiving 15 mg/kg MCEVs, and a group receiving 30 mg/kg MCEVs. After the induction of UC, the treated groups were orally administered varying concentrations of MCEVs for 5 days starting on day 6, while the control and DSS groups received an equal volume of PBS. The body weight, activity levels, and fecal status of mice were monitored daily, with colon and fecal samples collected on day 11 (Fig. 8A). The control group mice's body weights remained stable over the 11 days, while those in other groups decreased during the modeling process. Following 5 days of MCEVs administration, the 15 mg/kg MCEVs group did not show a notable variance in comparison to the DSS group. However, the body weights of the mice in the 30 mg/kg MCEVs group began to increase on the third day after MCEVs administration, and by day 11, their body weight was notably higher than that of the DSS group (Fig. 8B). Shortening of the colon is a crucial factor in assessing the disease severity [33]. Measurements of mean colon lengths in the four groups revealed lengths of 7.1 cm (control), 5.4 cm (DSS), 6.25 cm (15 mg/kg MCEVs), and 6.73 cm (30 mg/kg MCEVs). The colon length of the DSS group was reduced by 23.9% in comparison to the control group, indicating successful modeling of UC. Additionally, mice treated with both concentrations of MCEVs exhibited significantly longer colons than those in the DSS group (Fig. 8C, D). Endoscopic observation was conducted following a 12-hour fasting period on day 11. The control group mice possessed healthy and smooth colonic tissues characterized by intact and clear capillaries and more transparent mucus in the intestinal lumen. In contrast, the DSS group displayed colonic tissues with numerous ulcerative lesions and blurred capillaries. However, the colonic tissues in the groups receiving 15 mg/kg and 30 mg/kg MCEVs treatment showed structural integrity, clear capillaries, and fewer or no ulcers, with the 30 mg/kg MCEVs group resulting in a healthier intestinal lumen (Fig. 8E).

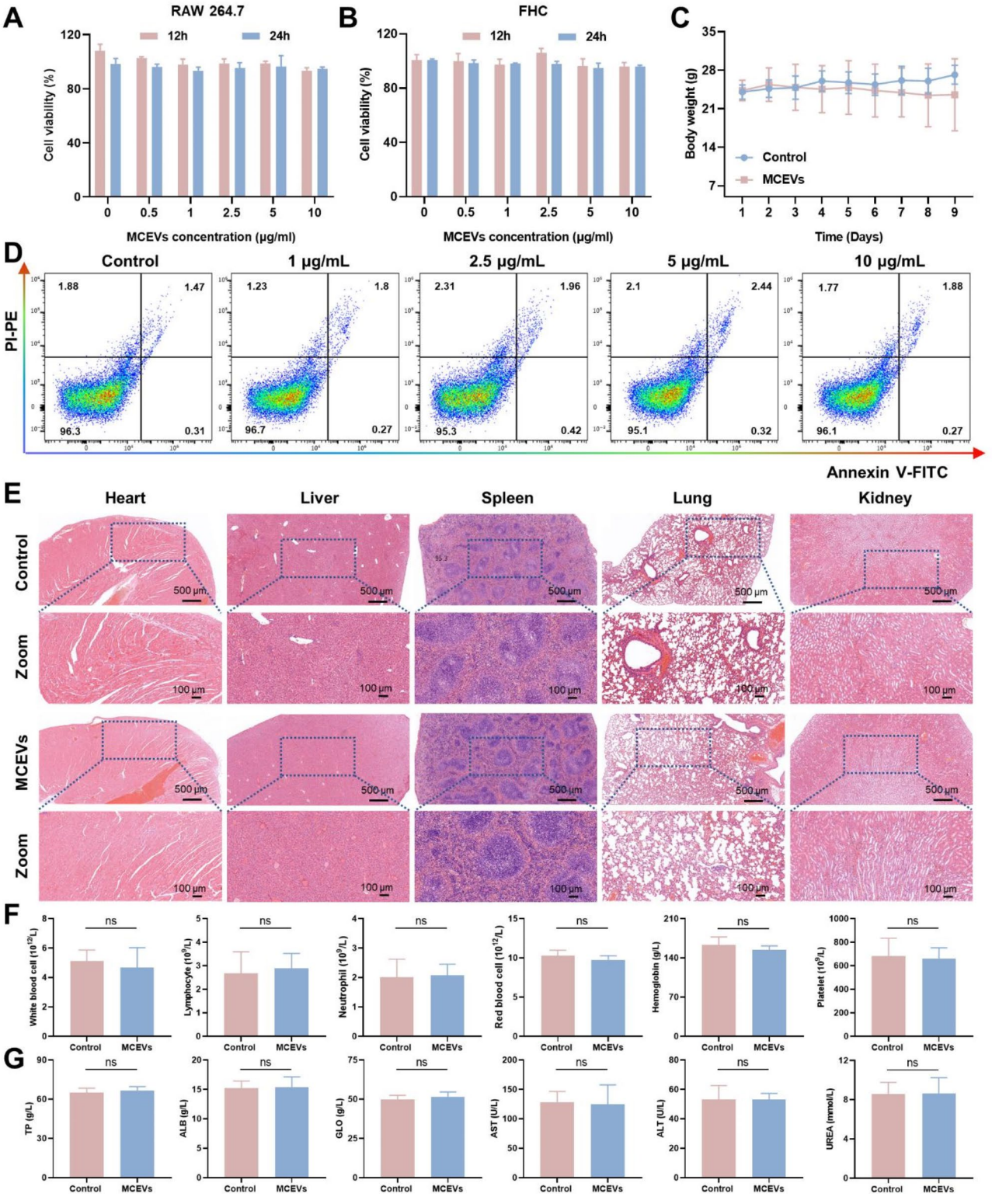

Fig. 6 Biocompatibility evaluation of MCEVs. Cell viability was evaluated using the MTT assay after co-incubation with MCEVs for 12 h and 24 h in **(A)** RAW264.7 and **(B)** FHC cells. **(C)** Body weight change of mice that were gavaged with PBS and MCEVs for 7 days and were killed on day 9. Mice were gavaged with equivalent PBS as control. **(D)** Apoptosis analysis of cells after co-incubated with MCEVs for 24 h by flow cytometry. **(E)** Histological analysis of vital organs isolated from the mice on day 9 by H&E staining. **(F)** The blood routine assays. **(G)** The biochemical assays. Data were shown as mean ± SD. $n \geq 3$, *: $P < 0.05$, **: $P < 0.01$, ***: $P < 0.001$, ns: $P > 0.05$, indicating no significance

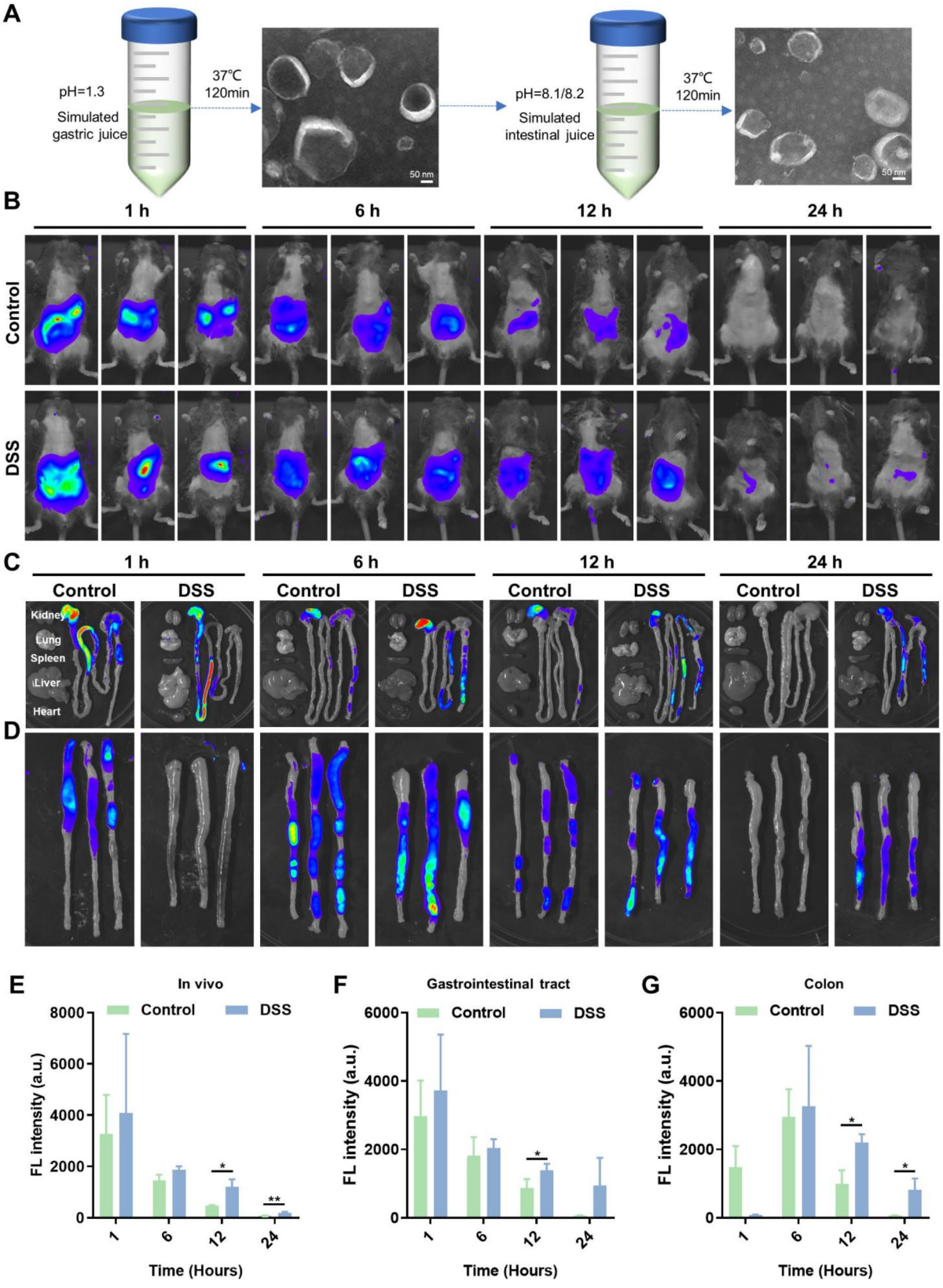

Fig. 7 Stability and biodistribution of MCEVs after oral administration. **(A)** TEM images of MCEVs after co-incubation with simulated gastric and simulated intestinal juice. **(B-D)** Fluorescence images of control and DSS-induced UC mice, organs, gastrointestinal tract, and colon at various time points after gavaged with DiR-labeled MCEVs. **(E-G)** Statistical analysis of relative fluorescence intensity in vivo, in the gastrointestinal tract and the colon at various time points. Data were shown as mean ± SD. $n \geq 3$, *: $P < 0.05$, **: $P < 0.01$, ***: $P < 0.001$, ns: $P > 0.05$, indicating no significance

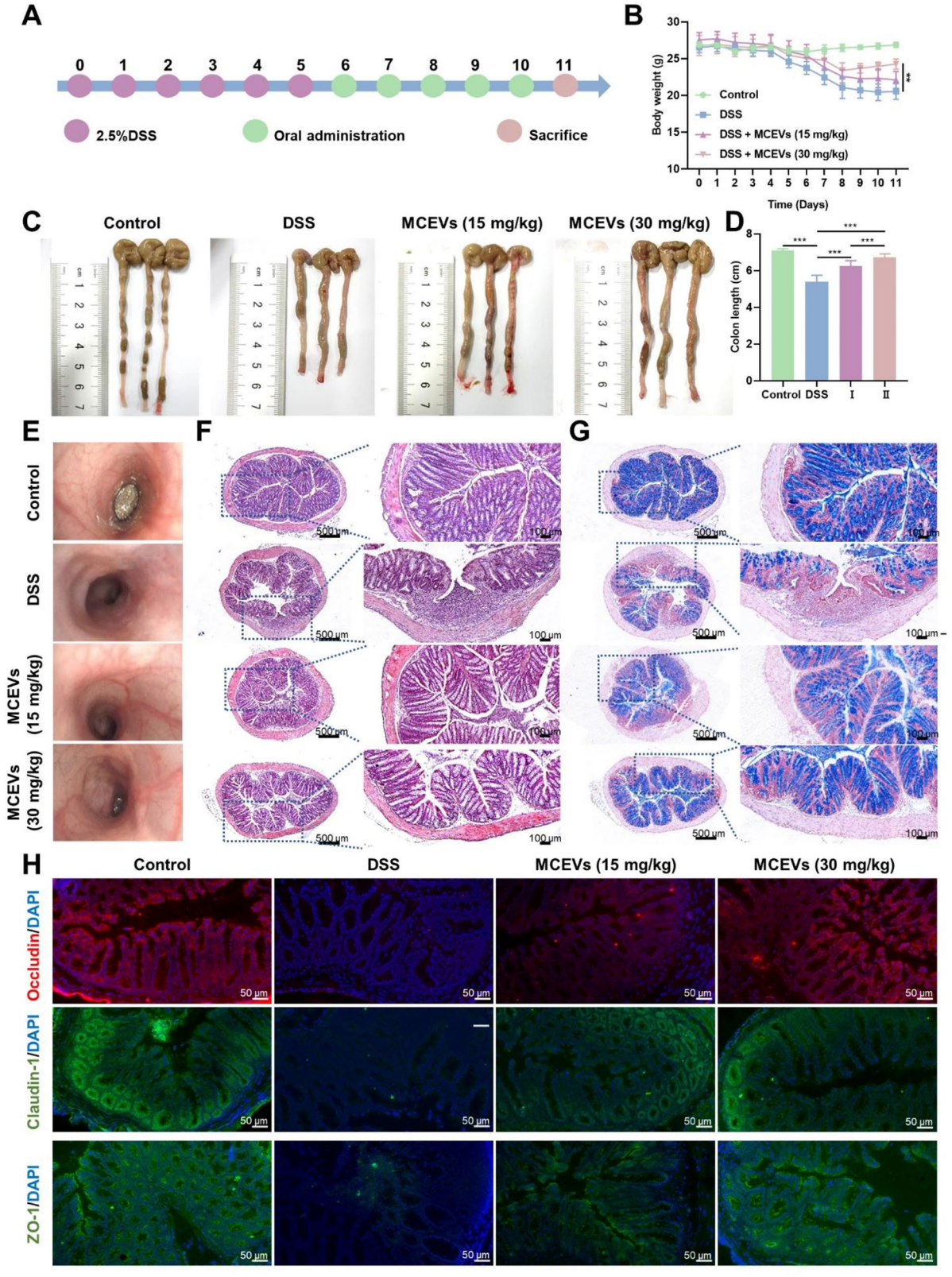

Fig. 8 (See legend on next page.)

(See figure on previous page.)

Fig. 8 Evaluation of the therapeutic effect of MCEVs on UC. **(A)** Schematic illustration of the establishment of a DSS-induced UC model and therapeutic strategies of MCEVs. **(B)** Body weight change chart of control, DSS, DSS + MCEVs 15 mg/kg, and DSS + MCEVs 30 mg/kg four groups of mice during 11 days ($n = 6$). **(C, D)** Comparison of colon length of four groups on day 11. ($n = 6$, I: DSS + MCEVs 15 mg/kg II: DSS + MCEVs 30 mg/kg). **(E)** Representative endoscopic images of four groups of mice on day 11. **(F)** Histological assessment of the mid-colon sections using H&E staining. **(G)** Alcian Blue staining of the mid-colon sections to evaluate mucin secretion. **(H)** Immunofluorescence photographs of tight junction protein to assess colon epithelial layer integrity. Data were shown as mean ± SD. *: $P < 0.05$, **: $P < 0.01$, ***: $P < 0.001$, ns: $P > 0.05$, indicating no significance

Intestinal barriers consist of biological, mucosal, mechanical, and immune components. The mucus layer exhibits adhesive and lubricating properties that impede the adherence of bacteria and other deleterious agents to the mucosa, thereby aiding in their expulsion. Intestinal epithelial cells act as a formidable barrier against the infiltration of bacteria, viruses, and endotoxins through tightly arranged intercellular junctions [34, 35]. We employed histological techniques, including H&E staining, Alcian blue staining, and immunofluorescence staining, to examine the restoration of the intestinal mucosa and physical barrier following intervention with MCEVs. H&E staining analysis revealed that control mice exhibited an intact colon structure without any abnormalities, while mice in the DSS group displayed pronounced inflammatory lesions characterized by the infiltration of inflammatory cells, crypt cysts, and disruption of the epithelial cell layer. Conversely, these inflammatory manifestations were notably ameliorated following intervention with MCEVs (Fig. 8F). Alcian blue staining results showed a significant decrease in mucin secretion in the DSS group, with a marked increase observed following MCEVs administration, suggesting enhanced goblet cell number and function within the crypts and substantial restoration of the mucosal barrier (Fig. 8G). Immunofluorescence staining results indicated a significant reduction in the expression of tight junction proteins Occludin, Claudin-1, and ZO-1 in the DSS group, with an increase observed following the administration of MCEVs. Additionally, the group receiving 30 mg/kg MCEVs exhibited restoration of tight junction protein expression closest to that of the control group, suggesting the potential of MCEVs to effectively promote structural integrity in the colon (Fig. 8H). These findings offered compelling evidence for the therapeutic efficacy of MCEVs in vivo.

The effects of mitigating inflammation of MCEVs in vivo

During the active phase of UC, a complex inflammatory environment characterized by immune cell infiltration is present in the lamina propria of the colon, leading to elevated levels of inflammation factors within the affected area [36]. To examine the extent of immune cell infiltration, colon tissue immune cells were extracted. The findings revealed a notable rise in the proportion of leukocytes in the DSS group, whereas a marked reduction was observed in the group treated with MCEVs (Fig. 9A, B). Neutrophils are the initial cells recruited during the flare-up phase of the disease and constitute the primary component of the inflammatory infiltrate in UC colon tissue. Flow cytometry findings indicated a statistically significant elevation in the leukocyte neutrophil percentage within the DSS group in comparison to the control group. Following MCEVs administration, there was a decrease in neutrophil percentage, with a more pronounced reduction observed at higher concentrations of MCEVs (Fig. 9C, D).

Inflammatory factors and ROS have the potential to disturb the integrity of the colonic epithelial barrier. Maintaining inflammation and redox balance is essential for the successful recovery from UC [37]. High levels of myeloperoxidase (MPO) are a remarkable marker of neutrophil infiltration, which aggravates UC. Mice in the DSS group exhibited notably elevated MPO activity compared to the control group, which was subsequently reduced following treatment with MCEVs (Fig. 9E). This result was consistent with the findings shown in Figs. 8C and D. qRT-PCR was performed to analyze the levels of inflammatory factors in colon tissues. The findings indicated a notable rise in the transcription level of pro-inflammatory factors IL-6, IL-1β, and TNF-α in the DSS group. Subsequent administration of MCEVs via gavage suppressed the secretion of these pro-inflammatory factors, with a more pronounced effect observed at the higher concentration of 30 mg/kg compared to the lower concentration of 15 mg/kg. Additionally, a significant decrease in the transcription level of the anti-inflammatory factor IL-10 was observed in the DSS group, while MCEV administration elevated its transcription level (Fig. 9F). Therefore, MCEVs have the potential to act as anti-inflammatory agents by suppressing pro-inflammatory factor secretion. Ultimately, MCEVs may offer relief for UC by mitigating inflammatory and oxidative stress responses.

The effect of MCEVs on mice gut microbiota and metabolites

Mice with UC typically exhibit dysbiosis in their intestinal microbiota, marked by decreased biodiversity, an imbalance between beneficial and pathogenic microorganisms, and changes in spatial distribution [38]. To delve deeper into the regulatory impacts of MCEVs on the intestinal microbiota, we extracted intestinal contents from the therapeutic model mice and analyzed the intestinal microbiota utilizing 16 S rRNA gene sequences.

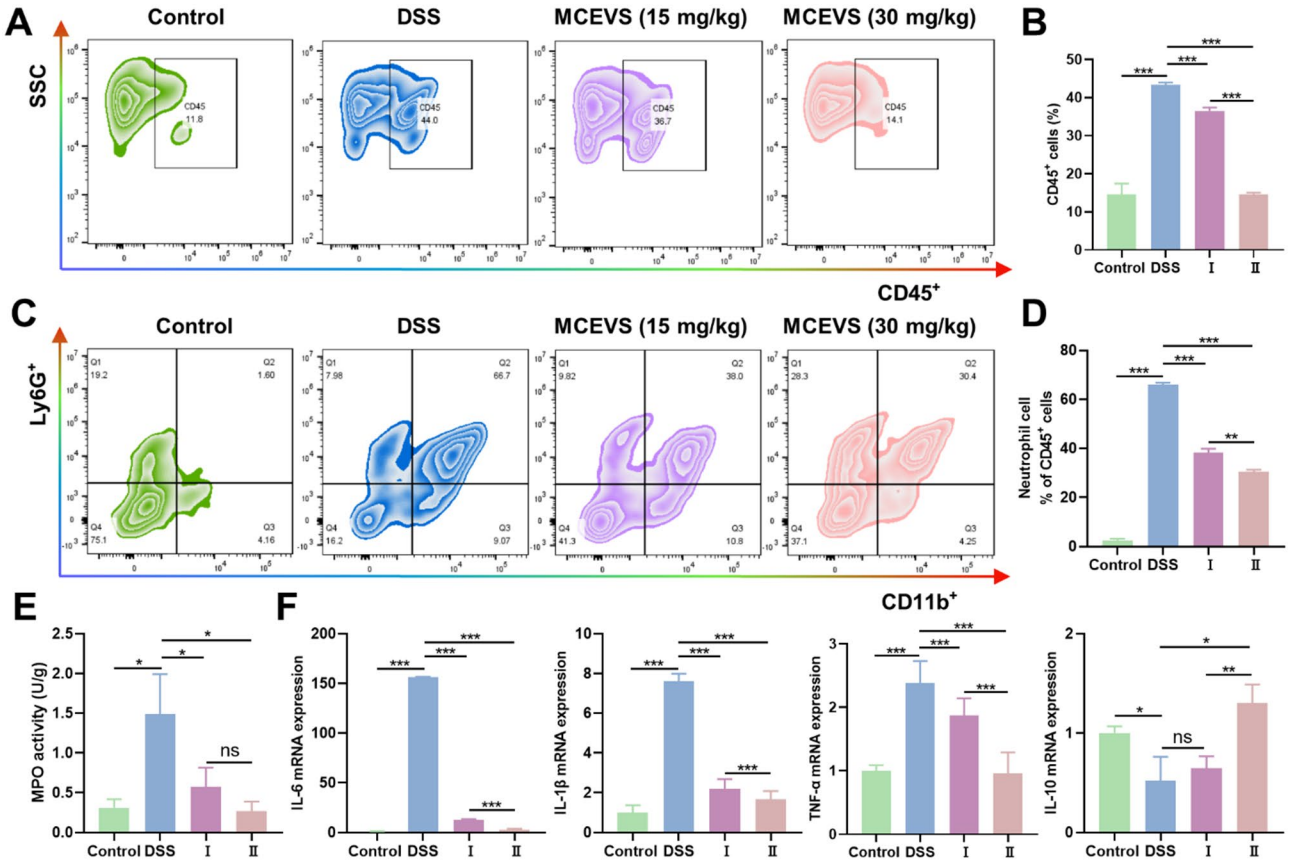

Fig. 9 The effects of mitigating inflammation of MCEVs in vivo. **(A, B)** Representative scatterplot and statistical chart of the percentage of leucocytes in the colon after oral administrated with MCEVs by Flow cytometry. **(C, D)** Representative scatterplot and statistical chart of the percentage of neutrophils in leucocytes after oral administrated with MCEVs by Flow cytometry. **(E)** Assessment of peroxidase activity in colonic tissues to evaluate inflammatory cell infiltration indirectly. **(F)** qRT-PCR to evaluate the transcription level of inflammatory cytokines in four groups. Data were shown as mean ± SD. $n \geq 3$, *: $P < 0.05$, **: $P < 0.01$, ***: $P < 0.001$, ns: $P > 0.05$, indicating no significance

Venn diagram analysis revealed significant disparities in species number across the three groups (Fig. 10A). Analysis of α-diversity, as measured by Chao1 and Shannon's diversity index, showed decreased bacterial diversity in the DSS group after modeling, with a notable increase in bacterial diversity in the MCEVs-treated group (Fig. 10B, C). Primary coordinate analysis (PCoA) demonstrated significant variations in gut microbial profiles among the three groups (Fig. 10D). Figure 10E displayed a bar graph illustrating the distribution of gut microbiota at the phylum level among various groups. The percentage of Verrucomicrobia was elevated in the DSS group, whereas the MCEVs group exhibited a significantly lower percentage than the DSS group. During IBD, an increased Firmicutes/Bacteroidota ratio is often observed, which may indicate the therapeutic efficacy [39]. Statistical results showed a significant rise in the Firmicutes/Bacteroidota ratio in the DSS group, whereas a decrease was observed in the MCEVs group, suggesting a beneficial therapeutic effect of MCEVs on UC (Fig. 10F). Subsequently, genus-level abundance analysis was conducted, revealing a significant increase in the potentially pathogenic genus *Escherichia-Shigella* in the DSS group. Following treatment with MCEVs, this abundance was significantly reduced. Conversely, the beneficial bacterial genera *Muribaculum* and *Alistipes* exhibited significant reductions in the DSS group but showed significant increases post-MCEVs administration (Fig. 10G).

The gut microbiota is recognized as a metabolic entity that plays a crucial role in extracting nutrients and energy from consumed food, as well as in generating various metabolites that interact with specific receptors to influence host metabolism [40]. One example is the ability of intestinal flora to metabolize tryptophan into indole derivatives, which contributes to the maintenance of intestinal homeostasis by supporting epithelial cell regeneration, enhancing intestinal barrier integrity, and modulating immune system homeostasis [41]. Untargeted metabolomics techniques were employed to analyze the intestinal contents, revealing a significant increase in products associated with the indole metabolic pathway following MCEVs administration. These

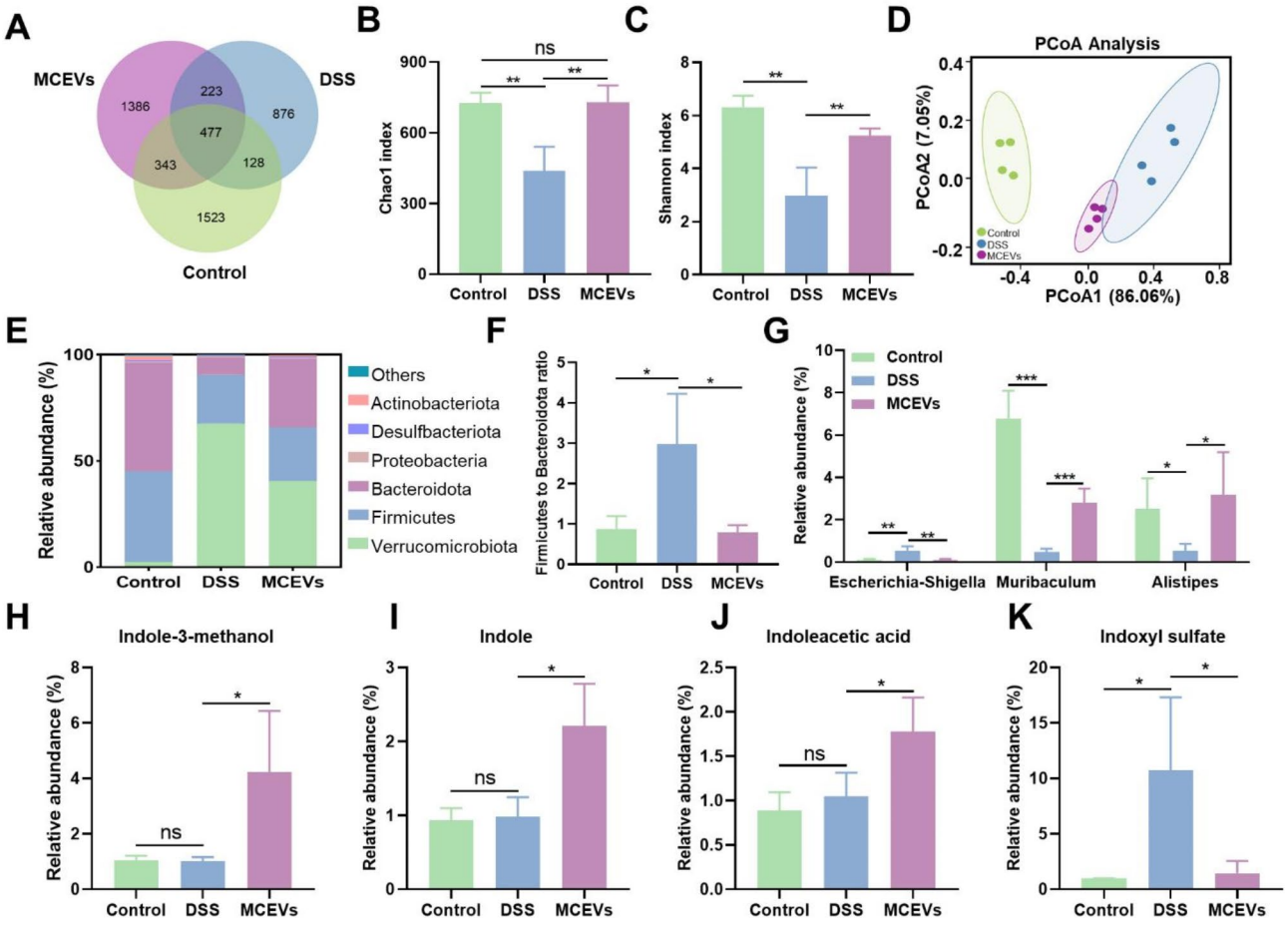

Fig. 10 The effect of MCEVs on mice gut microbiota and metabolites. **(A)** Venn diagram of common and unique bacterial species of intestinal contents among control, DSS, and DSS + MCEVs 30 mg/kg group. **(B-C)** Gut microbiota diversity was evaluated by the Chao 1 index and Shannon index. **(D)** Differential analysis of the composition of gut microbiota by principal coordinates analysis (PCoA). **(E)** Bar graph of microbiota abundance at the phylum level. **(F)** The ratio of Firmicutes/Bacteroidota. **(G)** The relative abundance of Escherichia-Shigella, Muribaculum, and Alistipes. **(H-K)** The relative content of indoles and derivatives was counted. **(H)** Indole-3-methanol, **(I)** Indole, **(J)** Indoleacetic acid, **(K)** Indoxyl sulfate. Data were shown as mean ± SD. $n \geq 3$, *: $P < 0.05$, **: $P < 0.01$, ***: $P < 0.001$, ns: $P > 0.05$, indicating no significance

products included Indole-3-methanol, Indole, and Indoleacetic acid (Fig. 10H-J). Indoxyl sulfate (IS) is a protein-bound toxin commonly metabolized by intestinal microorganisms. It leads to the inhibition of gene expression associated with transmembrane resistance and tight junctions in intestinal epithelial cells (IECs). This inhibition also impairs mitochondrial autophagy through the suppression of mitochondrial dynamin-related protein 1 (DRP1) expression, ultimately causing damage to the IECs [42]. Our experimental findings indicated a significant increase in IS levels in the DSS group, with an average relative content exceeding 10%. Following the administration of MCEVs, there was a notable decrease in IS content (Fig. 10K). In conclusion, these results suggested that MCEVs may alter intestinal metabolites by modulating the intestinal flora. These intestinal metabolites could be absorbed by epithelial cells to regulate cellular tight junction protein expression and enhance the intestinal physical barrier function, as well as regulate the intestinal immune system to maintain intestinal immune homeostasis.

The protective effect of MCEVs on UC

To enhance the credibility of the therapeutic effectiveness of MCEVs, four groups of mice were administered various intervention regimens during oral DSS induction (Fig. 11A). The experimental findings indicated that the group administered DSS exhibited a rapid decline in body weight and a sustained increase in disease activity index (DAI) throughout the experimental period. Treatment with a low dose (15 mg/kg) of MCEVs via gavage on alternate days did not result in significant differences in body weight changes compared to the DSS group. Conversely, mice receiving a high dose (30 mg/kg) of MCEVs demonstrated notable mitigation of the downward trend in body weight and elevation in DAI

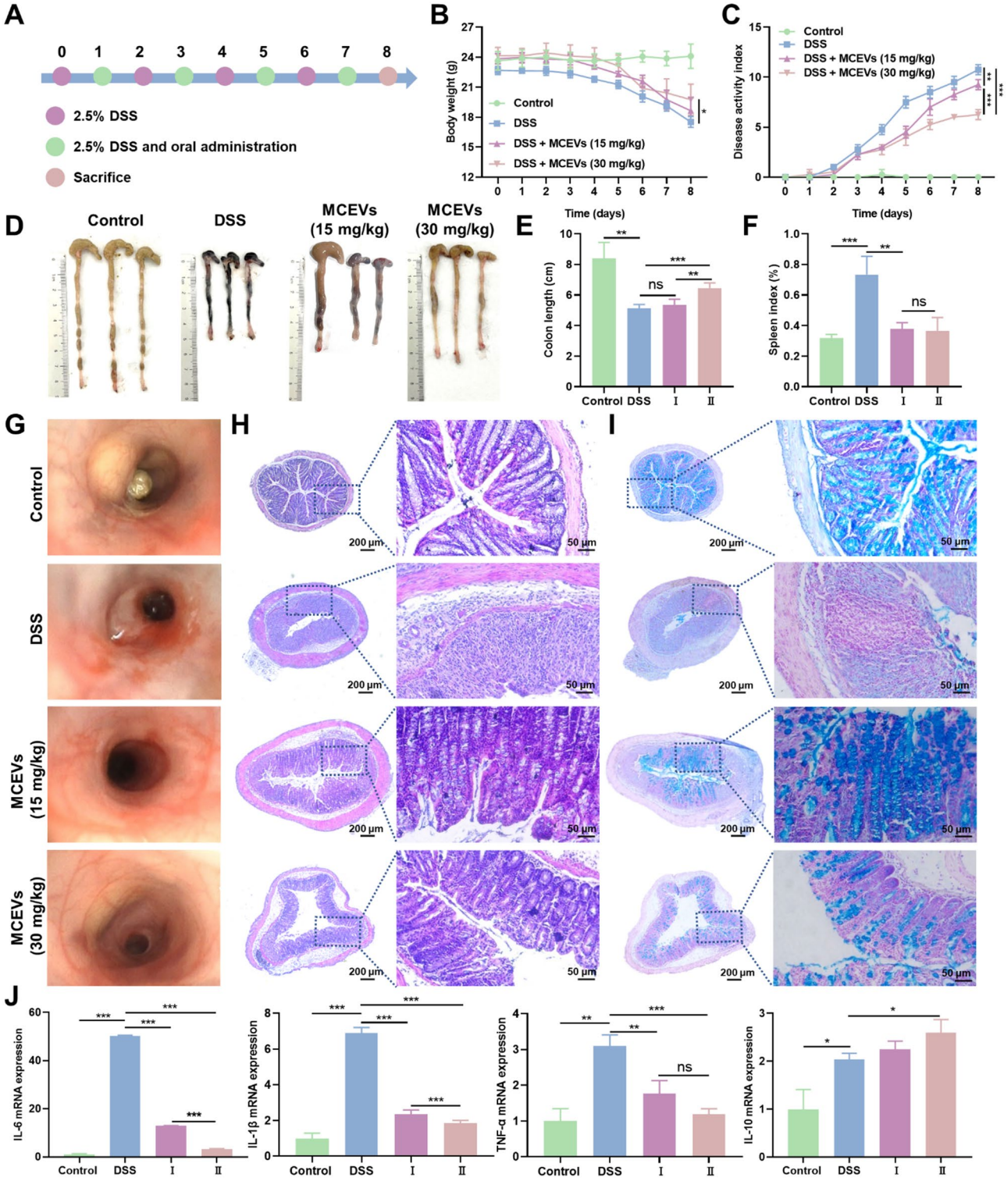

Fig. 11 Assessment of the protective effect of MCEVs on UC. **(A)** Schematic illustration of the establishment of a DSS-induced UC model and therapeutic strategies of MCEVs. **(B)** Body weight change chart of control, DSS, DSS + MCEVs 15 mg/kg, and DSS + MCEVs 30 mg/kg four groups of mice during 8 days ($n = 6$). **(C)** The Disease Activity Index (DAI) was recorded every day. **(D)** Representative images of the colon on day 8. **(E)** Comparison of colon length of four groups on day 8. **(F)** Comparison of spleen index of four groups on day 8. **(G)** Representative endoscopic images of four groups of mice on day 8. **(H)** Histological assessment of the mid-colon sections using H&E staining. **(I)** Alcian blue staining of the mid-colon sections to evaluate mucin secretion. **(J)** qRT-PCR to evaluate the transcription level of inflammatory cytokines. (I: DSS + MCEVs 15 mg/kg, II: DSS + MCEVs 30 mg/kg). Data were shown as mean ± SD. $n \geq 3$, *: $P < 0.05$, **: $P < 0.01$, ***: $P < 0.001$, ns: $P > 0.05$, indicating no significance

during DSS modeling (Fig. 11B, C). Colon length analysis revealed that the DSS group exhibited a marked reduction in average colon length after modeling. However, the group receiving MCEVs at 30 mg/kg exhibited a significantly greater colon length than the DSS group, suggesting that the higher dosage of MCEVs had a notable protective effect against DSS-induced ulcerative colitis (Fig. 11D, E). Following DSS modeling, the mice exhibited splenomegaly and reduced body weight, leading to a notable elevation in the splenic index. However, both low-dose and high-dose administrations of MCEVs effectively suppressed the DSS-induced increase in the splenic index (Fig. 11F). Endoscopy, H&E staining, and Alcian blue staining revealed that mice in the DSS group exhibited numerous hemorrhagic spots, submucosal edema, extensive infiltration of inflammatory cells into the intrinsic layer, disappearance of crypt structures, and epithelial cell layer rupture in the colon. Following oral administration of MCEVs, colonic hemorrhage was mitigated, inflammatory cell infiltration decreased, crypt structure was restored, goblet cell structure and function were normalized, and mucin secretion was markedly enhanced. The efficacy of gavage treatment with a high dosage of MCEVs was notably pronounced (Fig. 11G-I). Further, qRT-PCR results showed that MCEVs treatment reduced the secretion of pro-inflammatory factors induced by DSS modeling and promoted the secretion of anti-inflammatory factors, with a more significant effect observed at the higher 30 mg/kg concentration (Fig. 11J). Additionally, cells were extracted from mouse colon tissues for immunofluorescence flow cytometry analysis. The results showed that colon tissues exhibited severe immune cell infiltration after modeling, with more than 40% of leukocytes, more than half of which were neutrophils. Treatment with different doses of MCEVs significantly alleviated the inflammatory cell infiltration (Fig. S4). The aforementioned findings provide additional evidence supporting the favorable protective impact of MCEVs on the acute colitis mouse model induced by DSS.

Discussion

Plants serve as a valuable repository of natural medicines, and the current use of natural plants primarily involves extracting compounds from them. In recent years, numerous studies have shown that plant-derived extracellular vesicles (PDEVs) contain a large number of active substances that inherit the original pharmacological activities of plants [43], providing a new form for the development of natural plant-based therapies.

The utilization of PDEVs as therapeutic agents offers numerous advantages. These include the absence of detectable toxicity or immunogenicity in most edible plant cells, environmental friendliness due to their sustainable plant sources, ease and cost-effectiveness of cultivation and acquisition compared to human cell cultures, and freedom from human disease-causing pathogens [44]. Recent research has demonstrated that PDEVs exhibit promising therapeutic properties for various diseases, including IBD. For instance, lemon-derived extracellular vesicle nanomedicines have been shown to combat multidrug resistance in cancer cells by inducing endocytosis-mediated energy dissipation and inhibiting energy production [45]. Exosome-like nanovesicles derived from *Brucea javanica* have been found to deliver microRNAs for cancer treatment [46]. 'Green' nanotherapeutics extracted from plants such as tea leaves, ginger, mulberry bark, and turmeric show promise for managing colon diseases, including IBD and colitis-associated cancer, through targeted oral delivery and modulation of specific pathways. These studies have also verified that PDEVs exhibit remarkable stability, can withstand the challenging conditions of the gastrointestinal tract, and successfully reach the colon upon oral administration. They also demonstrate effective targeting and retention in models of IBD [47–50]. In this study, we confirmed the stability of MCEVs, remaining intact after 8 h of treatment with simulated gastric and simulated intestinal fluids. MCEVs also exhibited good retention in the UC colon, with the drug still present after 24 h rather than being rapidly metabolized following oral administration. These findings were consistent with those of previous related studies.

Various components from *Momordica charantia* have been demonstrated to exhibit anti-inflammatory and antioxidant effects. However, a single component from *Momordica charantia* has limited effects on the disease, and high concentrations of a single component may have side effects. Additionally, consuming large amounts of *Momordica charantia* to prevent IBD is impractical, which limits its clinical translation. MCEVs have emerged as novel nanotherapeutics for investigating the *Momordica charantia* medicinal style, expanding its potential therapeutic applications in disease management. Surprisingly, recent studies have shown that MCEVs exhibit significant efficacy in treating various diseases, suggesting their potential as therapeutic agents for clinical translation [15–19]. Our investigation further confirms the therapeutic effectiveness of MCEVs in a mouse model of DSS-induced acute UC. In addition, our findings suggest that MCEVs may improve intestinal epithelial barrier function by enhancing tight junctions and promoting mucus secretion. The potential mechanisms include ROS clearance, suppression of intestinal inflammatory cytokine expression and inflammatory cell infiltration, and maintenance of microbiome diversity.

Numerous studies have shown that the active small molecules in PDEVs play an essential role in disease

management. For example, curcumin in turmeric and ginsenosides in ginger have demonstrated therapeutic effects on UC [51, 52]. Similarly, extracellular vesicles derived from turmeric and ginger have also shown significant alleviating effects on colitis. Identification studies revealed that turmeric-derived vesicles contain curcumin, while ginseng-derived vesicles contain ginsenosides [48, 50]. In addition, it has been found that miRNAs in CHMEVs also have pharmacological activities. For instance, groundnut-derived extracellular vesicles carrying miR-7972 were shown to be the active ingredient for the anti-inflammatory activity of fresh groundnut, rather than catalpol and mullein, which are well-known active ingredients of groundnut [53]. Moreover, rowberry-derived extracellular vesicles delivered 10 functional miRNAs to 4T1 cells, promoting ROS/Caspase-mediated apoptosis through regulation of the Akt/mTOR signaling pathway. This significantly delayed the growth and metastasis of 4T1 cells [46]. Our results showed that RNA or protein digestion attenuated the inhibitory effect of MCEVs on inflammatory factor secretion, suggesting that proteins, RNA, and other classes of substances in MCEVs all contribute to their anti-inflammatory effect. Moving forward, we will continue to study to determine which specific proteins or RNA are pharmacologically active, thereby laying the theoretical foundation for advancing the clinical application of MCEVs.

Conclusion

In summary, a combination of differential centrifugation and density gradient centrifugation was utilized to isolate MCEVs. Our results revealed that MCEVs exhibited robust anti-inflammatory and antioxidant effects and could inhibit macrophage polarization and the secretion of inflammatory factors. Moreover, MCEVs were rich in bioactive contents, with proteins, RNA, and other compounds all contributing to their anti-inflammatory effects. Our findings suggested that MCEVs have the potential to mitigate mitochondrial oxidative stress induced by ROS in RAW 264.7 macrophage cells. They can preserve mitochondrial integrity and functionality, regulate the expression of apoptosis-related proteins, and consequently suppress mitochondria-mediated apoptosis. In vivo, orally administered MCEVs demonstrated good biosafety and colonic retention. Further, MCEVs showed efficacy in ameliorating symptoms associated with DSS-induced UC by suppressing ROS levels, reducing the secretion of inflammatory mediators, and restraining the inflammatory cell infiltration in colonic tissues. Additionally, our findings suggested that the therapeutic effects of MCEVs on UC also may be mediated by regulating the gut microbiota and its indole-related metabolites. Taken together, MCEVs preserved the inherent anti-inflammatory, antioxidant, and gut microbiota-regulating properties of *Momordica charantia*. This highlights their potential as a multi-target therapeutic approach for UC, which warrants further investigation to facilitate clinical implementation. Meanwhile, the extraction of extracellular vesicles that retain the pharmacological activity of the original plant provides a new strategy for the development of medicinal plants.

Supplementary Information

The online version contains supplementary material available at https://doi.org/10.1186/s12951-025-03346-6.

Supplementary Material 1

Acknowledgements

We thank Dr. Zijun Ren at the Instrument Analysis Center of Xi'an Jiaotong University for assisting with TEM analysis and Dr. Xiaofei Wang at the experimental biomedical center of Xi'an Jiaotong University for his kind assistance with the instrument operation and data analysis.

Author contributions

Bowen Gao: Investigation, Methodology, Data curation, Formal analysis, Software, Validation, Writing-original draft. Xioaling Huang: Investigation, Methodology. Junlong Fu: Conceptualization, Methodology, Formal analysis. Liyuan Chen: Data curation.Zhichao Deng: Writing-review & editing. Shuhui Wang: Data curation. Yuanyuan Zhu: Data curation. Chenxi Xu: Data curation. Yujie Zhang: Methodology. Mingxin Zhang: Methodology. Lina Chen: Conceptualization, Writing-review & editing, Supervision. Manli Cui: Conceptualization, Writing-review & editing, Supervision. Mingzhen Zhang: Conceptualization, Writing-review & editing, Supervision, Funding acquisition, and Project administration.

Funding

This work was supported by the National Natural Science Foundation of China (Nos. 82472127 and 82000823). The Fundamental Research Funds for the Central Universities, China (No. xtr052023008), and the Young Talent Support Plan of Xi'an Jiaotong University, China (No. YX6J001).

Data availability

No datasets were generated or analysed during the current study.

Declarations

Ethics approval and consent to participate

All work performed on animals was performed following the Guidelines for Care and Use of Laboratory Animals of Xi'an Jiaotong University and was approved by the Animal Ethics Committee.

Consent for publication

Not applicable.

Competing interests

The authors declare no competing interests.

Author details

[1]School of Basic Medical Sciences, Xi'an Jiaotong University, Xi'an, Shaanxi 710061, China
[2]Department of Gastroenterology, People's Hospital of Xinjiang Uygur Autonomous Region, Urumqi, Xinjiang Uygur Autonomous Region 830001, China
[3]Department of Gastroenterology, The Second Affiliated Hospital of Xi'an Jiaotong University, Xi'an, Shaanxi 710061, China
[4]Department of Gastroenterology, The First Affiliated Hospital of Xi'an Medical University, Xi'an, Shaanxi 710077, China

Received: 7 February 2025 / Accepted: 23 March 2025
Published online: 01 April 2025

References

1. Gilliland A, Chan JJ, De Wolfe TJ, Yang H, Vallance BA. Pathobionts in inflammatory bowel disease: origins, underlying mechanisms, and implications for clinical care. Gastroenterology. 2024;166:44–58.
2. Ng SC, Shi HY, Hamidi N, Underwood FE, Tang W, Benchimol EI, Panaccione R, Ghosh S, Wu JCY, Chan FKL, et al. Worldwide incidence and prevalence of inflammatory bowel disease in the 21st century: a systematic review of population-based studies. Lancet. 2017;390:2769–78.
3. Kobayashi T, Siegmund B, Le Berre C, Wei SC, Ferrante M, Shen B, Bernstein CN, Danese S, Peyrin-Biroulet L, Hibi T. Ulcerative colitis. Nat Rev Dis Primers. 2020;6.
4. Le Berre C, Honap S, Peyrin-Biroulet L. Ulcerative colitis. Lancet. 2023;402:571–84.
5. Forrester SJ, Kikuchi DS, Hernandes MS, Xu Q, Griendling KK. Reactive oxygen species in metabolic and inflammatory signaling. Circ Res. 2018;122:877–902.
6. Tian T, Wang Z, Zhang J. Pathomechanisms of oxidative stress in inflammatory bowel disease and potential antioxidant therapies. Oxid Med Cell Longev. 2017;2017:1–18.
7. Schirmer M, Franzosa EA, Lloyd-Price J, Mciver LJ, Schwager R, Poon TW, Ananthakrishnan AN, Andrews E, Barron G, Lake K, et al. Dynamics of metatranscription in the inflammatory bowel disease gut Microbiome. Nat Microbiol. 2018;3:337–46.
8. Rogler G. Resolution of inflammation in inflammatory bowel disease. Lancet Gastroenterol Hepatol. 2017;2:521–30.
9. Cui Y, Gao J, He Y, Jiang L. Plant extracellular vesicles. Protoplasma. 2019;257:3–12.
10. He W, Zheng S, Zhang H, Gao B, Jin J, Zhang M, He Q. Plant-Derived Vesicle-Like nanoparticles: clinical application exploration and challenges. Int J Nanomed. 2023;18:5671–83.
11. Fang Z, Liu K. Plant-derived extracellular vesicles as oral drug delivery carriers. J Control Release. 2022;350:389–400.
12. Cong M, Tan S, Li S, Gao L, Huang L, Zhang H-G, Qiao H. Technology insight: Plant-derived vesicles—How Far from the clinical biotherapeutics and therapeutic drug carriers? Adv Drug Deliver Rev. 2022;182.
13. Kwatra D, Dandawate P, Padhye S, Anant S. Bitter melon as a therapy for diabetes, inflammation, and cancer: a panacea?? Curr Pharmacol Rep. 2016;2:34–44.
14. Sur S, Ray RB. Diverse roles of bitter melon (< i > *Momordica charantia*) in prevention of oral cancer. J Cancer Metas Treat. 2021;2021.
15. Wang B, Guo X-J, Cai H, Zhu Y-H, Huang L-Y, Wang W, Luo L, Qi S-H. *Momordica charantia*-derived extracellular vesicles-like nanovesicles inhibited glioma proliferation, migration, and invasion by regulating the PI3K/AKT signaling pathway. J Funct Foods. 2022;90.
16. Cai H, Huang L-Y, Hong R, Song J-X, Guo X-J, Zhou W, Hu Z-L, Wang W, Wang Y-L, Shen J-G et al. *Momordica Charantia* Exosome-Like nanoparticles exert neuroprotective effects against ischemic brain injury via inhibiting matrix metalloproteinase 9 and activating the AKT/GSK3β signaling pathway. Front Pharmacol. 2022;13.
17. Feng T, Wan Y, Dai B, Liu Y. Anticancer activity of bitter Melon-Derived vesicles extract against breast cancer. Cells. 2023;12.
18. Yang M, Luo Q, Chen X, Chen F. Bitter melon derived extracellular vesicles enhance the therapeutic effects and reduce the drug resistance of 5-fluorouracil on oral squamous cell carcinoma. J Nanobiotechnol. 2021;19.
19. Cui W-W, Ye C, Wang K-X, Yang X, Zhu P-Y, Hu K, Lan T, Huang L-Y, Wang W, Gu B et al. Momordica. charantia-Derived extracellular Vesicles-Like nanovesicles protect cardiomyocytes against radiation injury via attenuating DNA damage and mitochondria dysfunction. Front Cardiovasc Med. 2022;9.
20. Van Niel G, D'angelo G, Raposo G. Shedding light on the cell biology of extracellular vesicles. Nat Rev Mol Cell Bio. 2018;19:213–28.
21. Mulcahy LA, Pink RC, Carter DRF. Routes and mechanisms of extracellular vesicle uptake. J Extracell Vesicles. 2014;3.
22. Hegarty LM, Jones G-R, Bain CC. Macrophages in intestinal homeostasis and inflammatory bowel disease. Nat Rev Gastro Hepat. 2023;20:538–53.
23. Jomova K, Raptova R, Alomar SY, Alwasel SH, Nepovimova E, Kuca K, Valko M. Reactive oxygen species, toxicity, oxidative stress, and antioxidants: chronic diseases and aging. Arch Toxicol. 2023;97:2499–574.
24. Czabotar PE, Lessene G, Strasser A, Adams JM. Control of apoptosis by the BCL-2 protein family: implications for physiology and therapy. Nat Rev Mol Cell Bio. 2013;15:49–63.
25. Redza-Dutordoir M, Averill-Bates DA. Activation of apoptosis signalling pathways by reactive oxygen species. Bba-Mol Cell Res. 2016;1863:2977–92.
26. Singh R, Letai A, Sarosiek K. Regulation of apoptosis in health and disease: the balancing act of BCL-2 family proteins. Nat Rev Mol Cell Bio. 2019;20:175–93.
27. Chen X, Xing X, Lin S, Huang L, He L, Zou Y, Zhang X, Su B, Lu Y, Zheng D. Plant-derived nanovesicles: harnessing nature's power for tissue protection and repair. J Nanobiotechnol. 2023;21.
28. Li X-Y, Meng L, Shen L, Ji H-F. Regulation of gut microbiota by vitamin C, vitamin E and β-carotene. Food Res Int. 2023;169.
29. Wei R-R, Lin Q-Y, Adu M, Huang H-L, Yan Z-H, Shao F, Zhong G-Y, Zhang Z-L, Sang Z-P, Cao L, et al. The sources, properties, extraction, biosynthesis, pharmacology, and application of lycopene. Food Funct. 2023;14:9974–98.
30. Sherriff JL, O'sullivan T A, Properzi C, Oddo J-L, Adams LA, Choline. Its potential role in nonalcoholic fatty liver disease, and the case for human and bacterial genes. Adv Nutr. 2016;7:5–13.
31. Schneider H, Braun A, Füllekrug J, Stremmel W, Ehehalt R. Lipid based therapy for ulcerative Colitis—Modulation of intestinal mucus membrane phospholipids as a tool to influence inflammation. Int J Mol Sci. 2010;11:4149–64.
32. Chen X, Liu B, Li X, An TT, Zhou Y, Li G, Wu-Smart J, Alvarez S, Naldrett MJ, Eudy J et al. Identification of anti-inflammatory vesicle-like nanoparticles in honey. J Extracell Vesicles. 2021;10.
33. Ungaro R, Mehandru S, Allen PB, Peyrin-Biroulet L, Colombel J-F. Ulcerative colitis. Lancet. 2017;389:1756–70.
34. Horowitz A, Chanez-Paredes SD, Haest X, Turner JR. Paracellular permeability and tight junction regulation in gut health and disease. Nat Rev Gastro Hepat. 2023;20:417–32.
35. Vancamelbeke M, Vermeire S. The intestinal barrier: a fundamental role in health and disease. Expert Rev Gastroent. 2017;11:821–34.
36. De Souza HSP, Fiocchi C. Immunopathogenesis of IBD: current state of the Art. Nat Rev Gastro Hepat. 2015;13:13–27.
37. Yao D, Dong M, Dai C, Wu S. Inflammation and inflammatory cytokine contribute to the initiation and development of ulcerative colitis and its associated cancer. Inflamm Bowel Dis. 2019;25:1595–602.
38. Franzosa EA, Sirota-Madi A, Avila-Pacheco J, Fornelos N, Haiser HJ, Reinker S, Vatanen T, Hall AB, Mallick H, Mciver LJ, et al. Gut Microbiome structure and metabolic activity in inflammatory bowel disease. Nat Microbiol. 2018;4:293–305.
39. Khan I, Ullah N, Zha L, Bai Y, Khan A, Zhao T, Che T, Zhang C. Alteration of gut microbiota in inflammatory bowel disease (IBD): cause or consequence?? IBD treatment targeting the gut Microbiome. Pathogens. 2019;8.
40. Wahlström A, Sayin Sama i, Marschall H-U, Bäckhed F. Intestinal Crosstalk between Bile Acids and Microbiota and Its Impact on Host Metabolism. Cell Metab. 2016;24:41–50.
41. Agus A, Planchais J, Sokol H. Gut microbiota regulation of Tryptophan metabolism in health and disease. Cell Host Microbe. 2018;23:716–24.
42. Vaziri ND, Zhao Y-Y, Pahl MV. Altered intestinal microbial flora and impaired epithelial barrier structure and function in CKD: the nature, mechanisms, consequences and potential treatment. Nephrol Dial Transpl. 2016;31:737–46.
43. Lian MQ, Chng WH, Liang J, Yeo HQ, Lee CK, Belaid M, Tollemeto M, Wacker MG, Czarny B, Pastorin G. Plant-derived extracellular vesicles: recent advancements and current challenges on their use for biomedical applications. J Extracell Vesicles. 2022;11.
44. Feng J, Xiu Q, Huang Y, Troyer Z, Li B, Zheng L. Plant-Derived Vesicle-Like nanoparticles as promising biotherapeutic tools: present and future. Adv Mater. 2023;35.
45. Xiao Q, Zhao W, Wu C, Wang X, Chen J, Shi X, Sha S, Li J, Liang X, Yang Y et al. Lemon-Derived extracellular vesicles nanodrugs enable to efficiently overcome cancer multidrug resistance by Endocytosis-Triggered energy dissipation and energy production reduction. Adv Sci. 2022;9.
46. Yan G, Xiao Q, Zhao J, Chen H, Xu Y, Tan M, Peng L. Brucea Javanica derived exosome-like nanovesicles deliver MiRNAs for cancer therapy. J Control Release. 2024;367:425–40.
47. Zu M, Xie D, Canup BSB, Chen N, Wang Y, Sun R, Zhang Z, Fu Y, Dai F, Xiao B. 'Green' nanotherapeutics from tea leaves for orally targeted prevention and alleviation of colon diseases. Biomaterials. 2021;279.
48. Zhang M, Viennois E, Prasad M, Zhang Y, Wang L, Zhang Z, Han MK, Xiao B, Xu C, Srinivasan S, et al. Edible ginger-derived nanoparticles: A novel therapeutic approach for the prevention and treatment of inflammatory bowel disease and colitis-associated cancer. Biomaterials. 2016;101:321–40.

49. Sriwastva MK, Deng ZB, Wang B, Teng Y, Kumar A, Sundaram K, Mu J, Lei C, Dryden GW, Xu F et al. Exosome-like nanoparticles from mulberry bark prevent DSS-induced colitis via the AhR/COPS8 pathway. Embo Rep. 2022;23.
50. Gao C, Zhou Y, Chen Z, Li H, Xiao Y, Hao W, Zhu Y, Vong CT, Farag MA, Wang Y, et al. Turmeric-derived nanovesicles as novel nanobiologics for targeted therapy of ulcerative colitis. Theranostics. 2022;12:5596–614.
51. Lin Y, Liu H, Bu L, Chen C, Ye X. Review of the effects and mechanism of Curcumin in the treatment of inflammatory bowel disease. Front Pharmacol. 2022;13.
52. Dong J-Y, Xia K-J, Liang W, Liu L-L, Yang F, Fang X-S, Xiong Y-J, Wang L, Zhou Z-J, Li C-Y, et al. Ginsenoside Rb1 alleviates colitis in mice via activation of Endoplasmic reticulum-resident E3 ubiquitin ligase Hrd1 signaling pathway. Acta Pharmacol Sin. 2020;42:1461–71.
53. Qiu F-S, Wang J-F, Guo M-Y, Li X-J, Shi C-Y, Wu F, Zhang H-H, Ying H-Z, Yu C-H. Rgl-exomiR-7972, a novel plant Exosomal MicroRNA derived from fresh rehmanniae radix, ameliorated lipopolysaccharide-induced acute lung injury and gut dysbiosis. Biomed Pharmacother. 2023;165.

Publisher's note